We are IntechOpen, the world's leading publisher of Open Access books
Built by scientists, for scientists

6,900
Open access books available

186,000
International authors and editors

200M
Downloads

Our authors are among the

154
Countries delivered to

TOP 1%
most cited scientists

12.2%
Contributors from top 500 universities

CLARIVATE ANALYTICS
BOOK CITATION INDEX
INDEXED

WEB OF SCIENCE™

Selection of our books indexed in the Book Citation Index
in Web of Science™ Core Collection (BKCI)

Interested in publishing with us?
Contact book.department@intechopen.com

Numbers displayed above are based on latest data collected.
For more information visit www.intechopen.com

Thermodynamic Properties of Ionic Liquids

Liu Qingshan, Mou Lin, Zheng Qige and Xia Quan

Additional information is available at the end of the chapter

Abstract

Basic physicochemical properties were discussed at different temperatures for 18 hydrophobic ionic liquids (ILs) which containing imidazolium and pyridinium as cations, separately. The ILs include 1-ethyl-3-methylimizazolium tris(pentafluoroethyl)trifluorophosphate ([C$_2$mim][PF$_3$(CF$_2$CF$_3$)$_3$]), 1-acetonitrile-3-ethylimimdazolium bis(trifluoromethylsulfonyl) imide ([MCNMIM][NTf$_2$]), 1-(cyanopropyl)-3-methylimidazolium bis[(trifluoromethyl)sulfonyl] imide [PCNMIM][NTf$_2$], 1-ethanol-3-ethylimimdazolium bis(trifluoromethylsulfonyl)imide ([EOHMIM][NTf$_2$]), 1-butylamide-3-ethylimimdazolium bis(trifluoromethylsulfonyl)-imide ([CH$_2$CONHBuEIM][NTf$_2$]), N-alkylpyridinium bis(trifluoromethylsulfonyl)imide {[C$_n$py][NTf$_2$] (n = 2, 3, 4, 5, 6)}, N-alkyl-3-methylpyridinium bis(trifluoromethyl-sulfonyl)imide {[C$_n$3Mpy][NTf$_2$] (n = 3, 4, 6)}, and N-alkyl-4-methylpyridinium bis(trifluoromethylsulfonyl) imide {[C$_n$4Mpy][NTf$_2$] (n = 2, 4, 6)}. The molar volume, standard molar entropy, and lattice energy were estimated by the empirical and semiempirical equations. The dependences of density, dynamic viscosity, and electrical conductivity on temperature are discussed in the measured temperature range. It is found that with the increasing temperature, the density and dynamic viscosity decreased, while the electrical conductivity increases. The influences of microstructures of ILs, such as the introduction of the methylene, methyl, and functional groups on cations, on their basic physicochemical properties are discussed.

Keywords: ionic liquid, density, surface tension, dynamic viscosity, electrical conductivity

1. Introduction

Ionic liquids (ILs) are salts while can exist as liquid at room temperature or near room temperature, which are completely composed of ions [1–3]. Compared with traditional organic solvents, ILs have exhibited outstanding properties, such as negligible vapor pressures, nonflammable, wide electrochemical window, high electrical conductivity, adjustable acidity, high dissolving

capacity for inorganic and organic compounds or polymers and can be recycled, etc. Moreover, ILs can be designed through the introduction of functional groups on anion or cation to modify their physicochemical properties. As the new designed and functional solvents, ILs have been used in fields of synthesis, extraction, catalysis, electrochemistry, etc. The basic physicochemical properties of ILs are of great importance for their design and applications; however, related data are very deficient. Therefore, IL's properties and related theoretical studies have received increasing attention.

2. Preparation of ionic liquids

All ionic liquids (ILs) were synthesized according to the reported method [4] except [CH$_2$CON HBuEIM][NTf$_2$] and [C$_2$mim][PF$_3$(CF$_2$CF$_3$)$_3$].

The chloride (or bromide) type compounds were synthesized by the N-alkylation reaction. A slight excess of halide was added dropwise into N-alkyl compounds by stirring at 353 K for 24 h. The products were recrystallized from acetonitrile/ethyl acetate solution several times. The products were dried under high vacuum for 48 h at 353 K before the synthesis of the target products. The [C$_2$mim][PF$_3$(CF$_2$CF$_3$)$_3$] was supplied by Merck Co. (batch: S9588301). The compound [CH$_2$CONHBuEIM][NTf$_2$] was synthesized according to the reported method [5]. Chloroacetyl chloride was added to n-butylamine drop by drop in the same molar ratio in an ice bath. After completion of the reaction, the organic layer was separated then washed with ω(HCl) = 5% or ω (NaHCO$_3$) = 5% until the water layer became neutral. The product (chloro-acetyl-n-butylamine) was dried under vacuum conditions. Acetonitrile was chosen as a solvent, ethylimidazole was added to chloroacetyl-n-butylamine in a small excess molar ratio to allow the complete reaction of chloroacetyl-n-butylamine at 85°C for 18 h. The product was recrystallized twice with acetonitrile and ethyl acetate ester. The resulting product was vacuum dried to obtain pure [EimCH$_2$CONHBu]Cl.

The hydrophobic ILs were synthesized in the distilled water by the traditional ion exchange reaction. The chloride (or bromide) type compounds were placed in a flask and dissolved with distilled water, an equivalent amount of lithium bis[(trifluoromethyl)sulfonyl]imide (LiNTf$_2$) salt was also dissolved in distilled water and added to the flask. The solution was stirred vigorously for 3 h. The bottom liquid was washed with distilled water until no halogen as detected by AgNO$_3$/ HNO$_3$ solution (the mass fraction of halogen was reckoned to be less than 50 ppm). The products were finally dried on vacuum drying line at 353 K before the determination of the thermodynamic properties. The final products were characterized by ^{1}H NMR spectra.

3. Water content

The impurity of the water is the most serious influence factor to the properties of ILs. Since the residual water cannot be removed by conventional methods in the ILs. The mass fraction of the residual water was determined by a Cou-Lo Aquamax Karl Fischer moisture meter (v.10.06)

before and after the measurement of properties. The water mass fractions of the ILs are lower than 300×10^{-6} and 500×10^{-6} for before and after the property determination, respectively.

4. Property measurement

4.1. Density

The densities of ILs were measured by a Westphal balance (or an automated SVM3000 Anton Paar rotational Stabinger viscometer-densimeter with a cylinder geometry) in the temperature range of $T = (283.15 \text{ to } 338.15) \pm 0.05$ K. The density values were recorded at every 5 K. For the Westphal balance method, the sample was placed in a cell with a jacket.

4.2. Surface tension

Using the tensiometer (DP-AW type produced by Sang Li Electronic Co.) of the forced bubble method, the surface tension of the ILs was measured with the experimental error that is ± 0.1 mJ·m^{-2}. The temperature was controlled by a thermostat. The uncertainties of the measurement are in the range of ± 0.2 mJ·m^{-2}.

4.3. Dynamic viscosity

The dynamic viscosity of the ILs was measured using an Ostwald viscometer (or an automated SVM3000 Anton Paar rotational Stabinger viscometer-densimeter with a cylinder geometry, the principle is based on a modified Couette according to a rapidly rotating outer tube and a relatively slow rotating inner measuring bob). The values were recorded at every 5 K. The uncertainties were estimated to be $\pm 1\%$.

4.4. Electrical conductivity

The electrical conductivity of the ILs was carried out using a MP522 conductivity instrument with the cell constants of 1 cm^{-1} (the cell was calibrated with the aqueous KCl solution). The uncertainty was reckoned to less than $\pm 1\%$. The temperature was regulated by a thermostat with a precision of ± 0.05 K. The experimental data were reported per 5 K after 30 min thermal equilibrium time.

5. Formulas

5.1. Density

A straight line can be obtained according to plot $\ln\rho$ against T/K. And the $\ln\rho$ against T/K can be fitted by the following empirical equation:

$$\ln\rho/\text{g} \cdot \text{cm}^{-3} = b - \alpha T/\text{K} \tag{1}$$

where b is an empirical constant and α is the thermal expansion coefficient.

At 298.15 K, the molecular volume, V, standard molar entropy, S^0, and lattice energy, U_{POT}, of the ILs can be obtained from the experimental density by the following equations:

$$V = M/(N \cdot \rho) \tag{2}$$

$$S^0 = 1246.5 \cdot (V) + 29.5 \tag{3}$$

$$U_{POT} = 1981.2 \cdot (\rho/M)^{1/3} + 103.8 \tag{4}$$

where M is molar mass, ρ is the density, and N is the Avogadro's constant.

5.2. Surface tension

The surface tension, γ, has the relationship with the temperature in terms of the Eötvös equation:

$$\gamma V^{2/3} = k(T_c - T) \tag{5}$$

where V is the molar volume of the liquid, T_c, is the critical temperature, and k, is an empirical constant.

The parachor, P, was estimated by the following equation:

$$P(298.15\,\mathrm{K}) = (M\,\gamma^{1/4})/\rho \tag{6}$$

where M is molar mass, ρ is the density, and γ is surface tension.

The molar enthalpy of vaporization, $\Delta_l^g H_m^0$, was estimated by the following equation:

$$\Delta_l^g H_m^0(298.15\mathrm{K})/\mathrm{kJ} \cdot \mathrm{mol}^{-1} = 0.01121(\gamma\, V^{2/3}\, N^{1/3}) + 2.4 \tag{7}$$

where V is molar volume, γ is surface tension, and N is Avogadro's constant.

At 298.15 K, according to the literature studies [6, 7], the interstice volume, v, can be estimated by interstice model theory:

$$v = 0.6791\,(k_b\, T/\gamma)^{3/2} \tag{8}$$

herein, k_b is the Boltzmann constant, T is thermodynamic temperature, and γ is the surface tension of ILs.

According to Yang et al., the molar volume of ILs is composed of the volume of inherent and interstices; herein, the molar volume of the interstice is, $\sum v = 2Nv$, the molar volume of the ILs can be calculated by the following equation:

$$V = V_i + 2Nv \tag{9}$$

herein, V is the molar volume, V_i is the inherent volume, and $2Nv$ is the interstice volume.

At 298.15 K, Yang et al. pointed out that the expansion volume of ILs only results from the interstices expansion following the temperature increase. Then, the thermal expansion coefficient, α, can be estimated by the interstice model theory by the following equation:

$$\alpha = (1/V)(\partial V/\partial T)_p = 3Nv/VT \tag{10}$$

5.3. Dynamic viscosity

The temperature dependence of the dynamic viscosity for ILs can be fitted using the Vogel-Fulcher-Tammann (VFT) equation:

$$\eta = \eta_0 \cdot \exp\left(B/\left(T - T_0\right)\right) \tag{11}$$

where η is the dynamic viscosity; η_0, B, and T_0 are the fitting parameters.

Usually, the Arrhenius equation was used to fit the dynamic viscosity and the equation is:

$$\eta = \eta_\infty \cdot \exp\left(E_\eta/\left(k_B T\right)\right) \tag{12}$$

where E_a is the activation energy for dynamic viscosity, η_∞ is the maximum dynamic viscosity, and k_B is the Boltzmann constant.

According to Vila et al. [12], the VFT equation for dynamic viscosity was related to the Arrhenius equation, $\eta_0 = \eta_\infty$ and $B = E_\eta/k_B$. The activation energy of dynamic viscosity was introduced in the final version VFT equation. The final version of the VFT equation can be expressed as follows:

$$\eta = \eta_\infty \cdot \exp(E_\eta/\left(k_B\left(T - T_0\right)\right) \tag{13}$$

5.4. Electrical conductivity

Usually, the VFT is also used for the fitting of temperature dependence on electrical conductivity. Herein, the temperature dependence of electrical conductivity of the ILs was also fitted according to the following VFT equation:

$$\sigma = \sigma_0 \cdot \exp\left(-B/\left(T - T_0\right)\right) \tag{14}$$

here σ is the electrical conductivity; σ_0, B, and T_0 are fitting parameters.

Sometimes, the Arrhenius equation is also used to fit the electrical conductivity:

$$\sigma = \sigma_\infty \cdot \exp\left(-E_\sigma / \left(k_B T\right)\right) \tag{15}$$

where E_σ is the activation energy, which indicates the energy needed for the ion to hop into a free hole, σ_∞ is the maximum electrical conductivity, and k_B is the Boltzmann constant.

According to the discussion, Vila et al. [8] have introduced the activation energy of electrical conductivity in the VFT equation by establishing the fitting parameters of the VFT equation with the Arrhenius equation: $\sigma_0 = \sigma_\infty$ and $B = E_\sigma / k_B$. The final version of the VFT equation can be expressed as follows:

$$\sigma = \sigma_\infty \cdot \exp\left(-E_\sigma / \left(k_B (T - T_0)\right)\right) \tag{16}$$

5.5. Walden rule

The classical Walden rule was usually used for the assessing of the ionicity of ILs [9, 10]. The ionic mobilities (represented by the equivalent conductivity $\Lambda = F\Sigma\mu_i Z_i$) and the fluidity ϕ ($\phi = \eta^{-1}$) of the medium can be related to the Walden rule through the ions move. On the basis of this fact, the relationship of the molar electrical conductivity and dynamic viscosity for ILs can be described by the following equation:

$$\Lambda\eta = k \tag{17}$$

where Λ is the molar electrical conductivity, η is the dynamic viscosity, and k is a temperature dependent constant. The Walden's product (in [S·cm²·mol⁻¹][mP·s]) can be calculated at 298.15 K.

6. Density and surface tension of ionic liquid [C₂mim][PF₃(CF₂CF₃)₃] and prediction of properties [Cₙmim][PF₃(CF₂CF₃)₃] (n = 1, 3, 4, 5, 6)

As organic salts, the ionic liquids (ILs) have shown many excellent properties, such as the low melting temperature, good solvation, and nonvolatility. So, the industrial and scientific communities have applied ILs in a broad range as the green organic solvents. In particular, the air- and water-stable hydrophobic ILs have been used in some special fields as the stable ILs. Actually, the most ILs are hydrophilic, so, 1-alkyl-3-methylimidazolium bis(trifluoromethylsulfonyl)imide (CₙmimNTf₂) has attracted serious concern as an air- and water-stable hydrophobic compound. And the properties were reporting in succession when the air- and water-stable hydrophobic compounds were synthesized. As another air- and water-stable hydrophobic type IL 1-ethyl-3-methylimizazolium tris(pentafluoroethyl)trifluorophosphate [C₂mim][PF₃(CF₂CF₃)₃] was provided by Merck Co. This is also the air- and water-stable hydrophobic IL. So, the study on the properties of this type ILs is significant in many concerned fields.

The structure of [C₂mim][PF₃(CF₂CF₃)₃] is shown in **Figure 1**.

The experimental measured values of density and surface tension of IL [C₂mim][PF₃(CF₂CF₃)₃] are listed in **Table 1** [11].
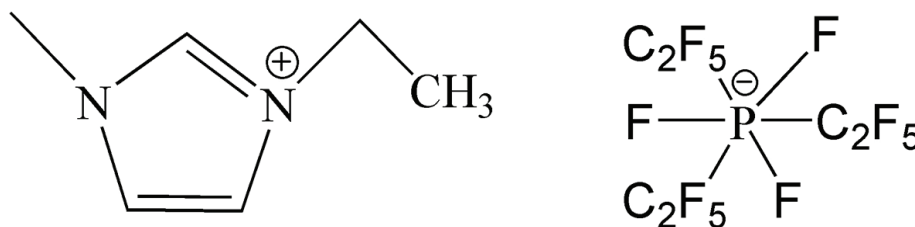
Figure 1. The structure of IL ([C_2mim][$PF_3(CF_2CF_3)_3$]).

T/K	283.15	288.15	293.15	298.15	303.15	308.15
ρ/g cm^{-3}	1.72705	1.72113	1.71517	1.70926	1.70332	1.69740
γ/mJ m^{-2}	35.3	35.1	34.9	34.8	34.6	34.4
T/K	313.15	318.15	323.15	328.15	333.15	338.15
ρ/g cm^{-3}	1.69150	1.68562	1.67975	1.67388	1.66804	1.66221
γ/mJ m^{-2}	34.2	34.1	34.0	33.8	33.6	33.4

Table 1. Experimental values of density, ρ, and surface tension, γ, of IL [C_2mim][$PF_3(CF_2CF_3)_3$] from 283.15 to 338.15 K.

By plotting ln ρ against (T − 298.15) K, a straight line can be obtained (see **Figure 2**) according to Eq. (1). According to Eq. (1), the correlation coefficient is $R = 0.9999$, the standard deviation $s = 3.0 \times 10^{-5}$ g cm^{-3}, $b = 0.53603$, the thermal expansion coefficient of the IL is $\alpha = 6.96 \times 10^{-4}$ K^{-1} at 298.15 K, respectively.
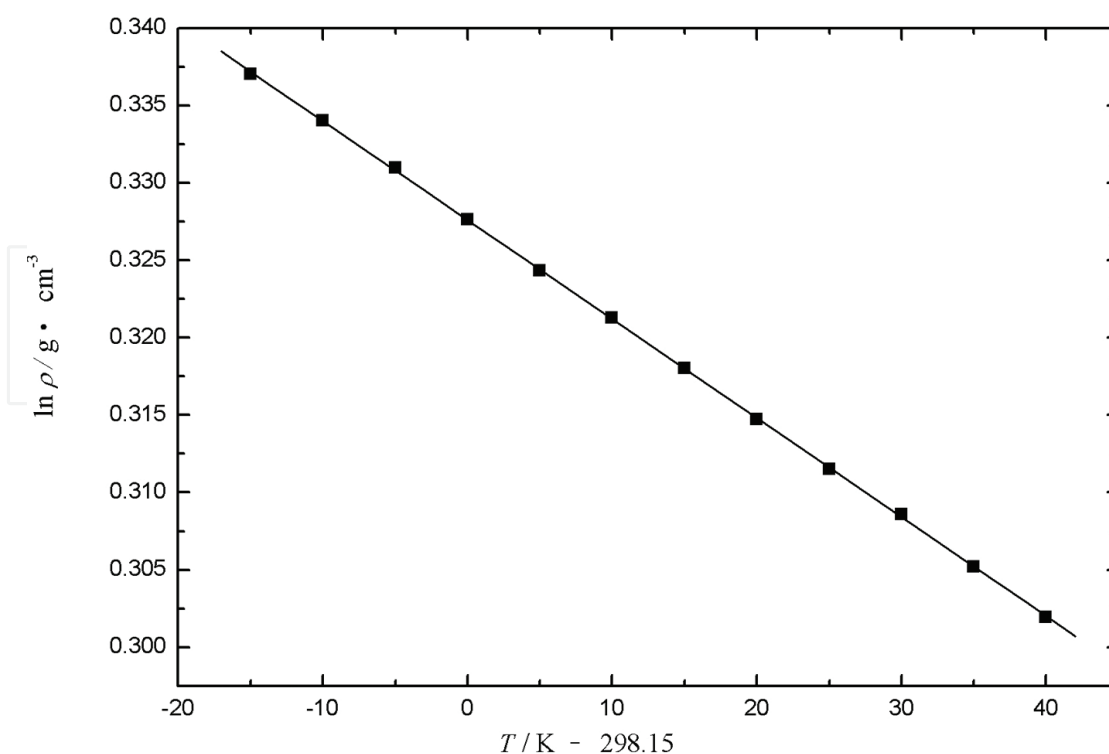

Figure 2. Plot of ln ρ vs. T/K − 298.15 of IL [C_2mim][$PF_3(CF_2CF_3)_3$].

The experiment values of γ against $(T - 298.15)$ K can be fitted according to the linear equation (see **Figure 3**). According to the linear equation, the correlation coefficient and standard deviation can be obtained and the values are 0.998 and 0.04 mJ·m^{-2}, respectively. In **Figure 3**, the surface entropy, $S_a = -(\partial\gamma/\partial(T - 298.15))_p$, can also be obtained and the value is 33.4×10^{-3} mJ·K^{-1}·m^{-2} at 298.15 K. At 298.15 K, the surface energy can be calculated from the surface tension value by the imperial equation, $E_a = \gamma - T(\partial\gamma/\partial(T - 298.15))_p$, and the value is 44.8 mJ·m^{-2}. Compared with surface energies of the fused salts and organic liquids, the value of the IL [C$_2$mim][PF$_3$(CF$_2$CF$_3$)$_3$] is close to the organic liquids, even less than some organic liquids, for example, 146 mJ·m^{-2} for NaNO$_3$, 67 mJ·m^{-2} for benzene, and 51.1 mJ·m^{-2} for octane. This fact shows that the interaction energy between ions in [C$_2$mim][PF$_3$(CF$_2$CF$_3$)$_3$] is less than that in fused salts. The physicochemical properties (molecular volume, V_m, parachor, P, thermal expansion coefficient, α, standard entropy, S^0, lattice energy, U_{pot}, and molar enthalpy of vaporization, $\Delta_l^g H_m^0$) were estimated by using the experimental data of density and surface tension according to Eqs. (1)–(7).
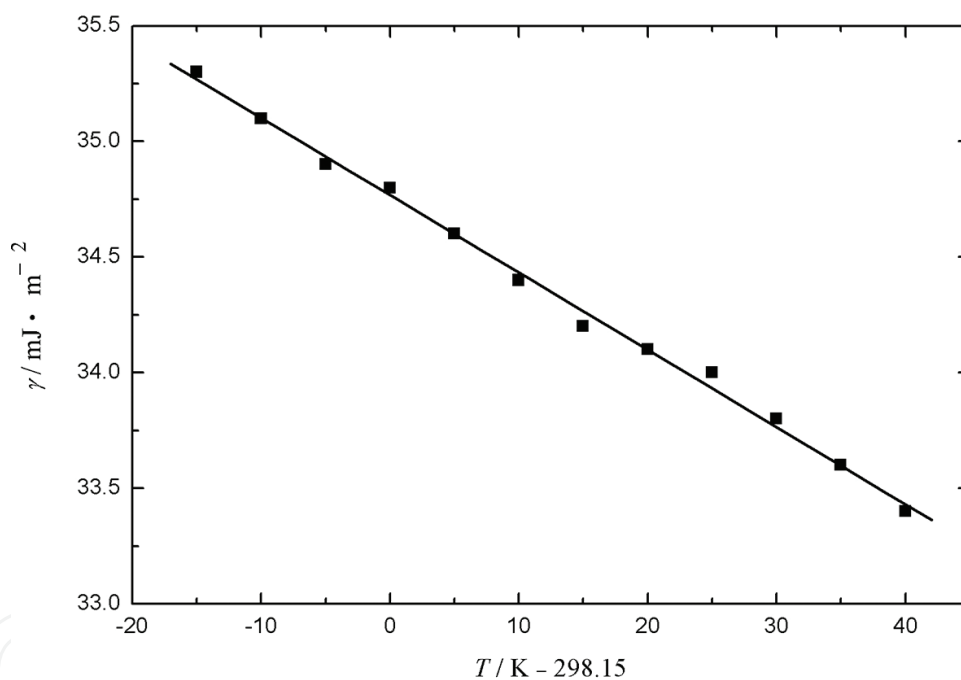

Figure 3. Plot of γ vs. T/K − 298.15 of IL [C$_2$mim][PF$_3$(CF$_2$CF$_3$)$_3$].

The contribution of the methylene (−CH$_2$−) group to the molecular volumes can be obtained according to the literature studies [12, 13]. The values of the ILs [C$_n$mim][BF$_4$], [C$_n$mim][NTf$_2$], [C$_n$mim][AlCl$_4$], and [C$_n$mim][Ala] are 0.0272, 0.0282, 0.0270 and 0.0278 nm^3, respectively. From the above values, the contribution of the methylene to the molecular volume can be considered to be similar. So, the mean value of the contribution can be calculated to be 0.0275 nm^3, the physicochemical properties (density, standard entropy, lattice energy) of the homologues of [C$_n$mim][PF$_3$(CF$_2$CF$_3$)$_3$] (n = 1, 3, 4, 5, 6) can be predicted. All of the predicted data are listed in **Table 2**.

Properties	[C$_1$mim] [PF$_3$(CF$_2$CF$_3$)$_3$] [p]	[C$_2$mim] [PF$_3$(CF$_2$CF$_3$)$_3$] [e]	[C$_3$mim] [PF$_3$(CF$_2$CF$_3$)$_3$] [p]	[C$_4$mim] [PF$_3$(CF$_2$CF$_3$)$_3$] [p]	[C$_5$mim] [PF$_3$(CF$_2$CF$_3$)$_3$] [p]	[C$_6$mim] [PF$_3$(CF$_2$CF$_3$)$_3$] [p]
M/g·mol^{-1}	542.15	556.18	570.20	584.23	598.26	612.29
V_m/nm^3	0.5130	0.5405	0.5680	0.5955	0.6230	0.6505
ρ/g·cm^{-3}	1.75552	1.70926 [m]	1.66756	1.62962	1.59516	1.56356
S^0/J·K^{-1}·mol^{-1}	669.0	703.3	737.5	771.8	806.1	840.3
U_{pot}/kJ·mol^{-1}	397	392	387	383	379	375
V/cm^{-3}·mol^{-1}	308.8	325.4	341.9	358.5	375.0	391.6
p	757.8	792.1	826.4	860.7	895.0	929.3
$\Delta_l^g H_m^0$/ kJ·mol^{-1}	161.9	157.8	160.3	161.1	162.0	163.1
$10^{24}v$/cm^3	25.93	27.63	28.48	29.65	30.75	31.78
$\sum v$/cm^3	31.22	33.33	34.29	35.70	37.03	38.26
$10^2\sum v/V$	10.11	10.22	10.29	9.96	9.87	9.77
$10^4\alpha$/K^{-1}		6.96 [m]				
$10^4\alpha$/K^{-1}	5.10	5.14	5.04	5.00	4.96	4.91
γ 10^3/N·m^{-1}	36.3	34.8 [m]	34.1	33.2	32.4	31.7

Notes: [m] measurement value; [p] data in the column were predicted values; [e] data in the column were estimated values.

Table 2. Estimated and predicted values of physicochemical properties of IL [C$_n$mim][PF$_3$(CF$_2$CF$_3$)$_3$] (n = 1, 2, 3, 4, 5, 6) at 298.15 K.

According to the literature [12, 13], the contribution per methylene (−CH$_2$−) to parachor is 31.1 for [C$_n$mim][AlCl$_4$] and 37.5 for [C$_n$mim][Ala]. An average value of the contribution can be calculated to be 34.3. So, the average value can be used to predict the parachor of the ILs [C$_n$mim][PF$_3$(CF$_2$CF$_3$)$_3$] (n = 1, 3, 4, 5, 6). According to Eq. (6), the surface tension can be calculated from the predicted density and parachor. The molar enthalpy of vaporization, $\Delta_l^g H_m^0$, can be obtained from the predicted density and surface tension. The data are listed in **Table 2**.

According to the predicted values of density and surface tension, the other properties can be predicted and the values are also listed in **Table 2**.

According to the interstice model and Eqs. (8)–(10) [6, 7], the interstice volume, v, the molar volume of ionic liquids, V, consists of the inherent volume, V_i, and the volume of the interstices; the molar volume of the interstice, $\sum v = 2Nv$, the thermal expansion coefficient, α, can be predicted from the interstice model at 298.15 K. All of the data obtained from estimation and prediction are listed in **Table 2**.

Table 2 shows the comparison of the predicted and experimental thermal expansion coefficients of [C$_2$mim][PF$_3$(CF$_2$CF$_3$)$_3$] at 298.15 K. The difference of the two values is about 26%. So, the predicted values of the expansion coefficient can be as the reference data when lack of reliable experimental values.

For the majority materials, the volume expansions are in the range of 10–15% from the solid state to the liquid state. From **Table 2**, the estimated and predicted interstice fractions are in the range of 9–11% for the serious ILs [$C_n$mim][PF$_3$(CF$_2$CF$_3$)$_3$] (n = 1, 2, 3, 4, 5, 6) at 298.15 K. The values are in good agreement with the reported values. Therefore, the interstice model theory can be used for calculation of the thermal expansion coefficient.

Conclusion

In this section, the density and surface tension of the imidazolium-type hydrophobic IL [C_2mim][PF$_3$(CF$_2$CF$_3$)$_3$] (n = 1, 2, 3, 4, 5, 6) were determined and predicted in the temperature range of 283.15–338.15 K. According to the estimated equations and interstice model theory, the thermodynamic properties of the serious ILs were calculated by the empirical and semiempirical equations at 298.15 K. The effect of the methylene on molecular volume and parachor was discussed and used for the prediction of the thermodynamic properties of ILs. From the predicted values of thermal expansion coefficient, the other predicted values can be used as the reference data when lack the reliable experimental values.

7. Density, dynamic viscosity, and electrical conductivity of imidazolium-type hydrophobic functional ionic liquids

Ionic liquids (ILs) have exhibited outstanding physicochemical properties, such as good solvation, negligible vapor pressure, good thermal stability, and designability. ILs have been used as the green solvents in industrial and scientific areas. The functional ionic liquids (FILs) have been paid much more attention because of the designability [14–24]. The physicochemical properties can be designed according to the introduction of the functional groups, such as −CN, −OH, and −CH$_2$-O-CH$_3$.

Egashira et al. [14–16] have introduced the cyano group on the imidazolium FILs and quaternary ammonium FILs, respectively. The FILs have been applied in the lithium batteries as electrolyte components. The FILs have showed an improved cycle behavior compared with the electrolyte based on a tetraalkylammonium ionic liquid without a cyano group. The quaternary ammonium-based FILs containing a cyano group showed the better stability of the cathodic than the imidazolium-based FILs. Hardacre et al. [17, 18] have also synthesized two series pyridinium type FILs. The effect of electron-withdrawing groups on the properties was discussed according to the presence of the nitrile or trifluoromethyl in this type FILs. The introduction of the two functional groups leads to the increasing of the melting temperature compared the traditional ILs. On the basis of this fact, the authors have observed the liquid charge-transfer complexes form upon contacting electron-rich aromatics with an electron withdrawing group appended 1-alkyl-4-cyanopyridinium ionic liquids. Zhang et al. [19] have studied the solubilities of C$_2$H$_4$ and CO$_2$ in the cyano-type imidazolium FILs using the gas chromatography. Compared with the 1,3-dialkylimidazolium-type ILs, the cyano-type FILs result in a remarkable decrease of the interactions of hydrocarbons. The cyano-type ILs have exhibited the advanta-

geous properties. As the solvent, it can be applied as a suitable reaction media and ligands in catalytic reactions, as an electrolyte in lithium batteries, as a solvent for extraction of metals and dissolution of cellulose.

Although the FILs have been applied in some areas, the physicochemical properties are not enough for the application [20–22]. In this chapter, the properties of 1-acetonitrile-3-ethylimimdazolium bis(trifluoromethylsulfonyl)imide [MCNMIM][NTf$_2$], 1-(cyanopropyl)-3-methylimidazolium bis[(trifluoromethyl)sulfonyl]imide [PCNMIM][NTf$_2$], 1-ethanol-3-ethylimimdazolium bis(trifluoromethylsulfonyl)imide [EOHMIM][NTf$_2$], 1-butylamide-3-ethylimimdazolium bis(trifluoromethylsulfonyl)-imide [CH$_2$CONHBuEIM][NTf$_2$] were compared with the traditional ILs 1-alkyl-3-mthylimimdazolium bis(trifluoromethylsulfonyl)imide [C$_n$MIM][NTf$_2$], (n = 2, 4) and 1-alkyl-2,3-dimthylimimdazolium bis(trifluoromethylsulfonyl)imide [C$_n$MMIM][NTf$_2$], (n = 2, 4).

The structure of [EMIM][NTf$_2$], [BMIM][NTf$_2$], [EMMIM][NTf$_2$], [BMMIM][NTf$_2$], [MCNMIM][NTf$_2$], [PCNMIM][NTf$_2$], [EOHMIM][NTf$_2$], and [CH$_2$CONHBuEIM][NTf$_2$] is shown in **Figure 4**.
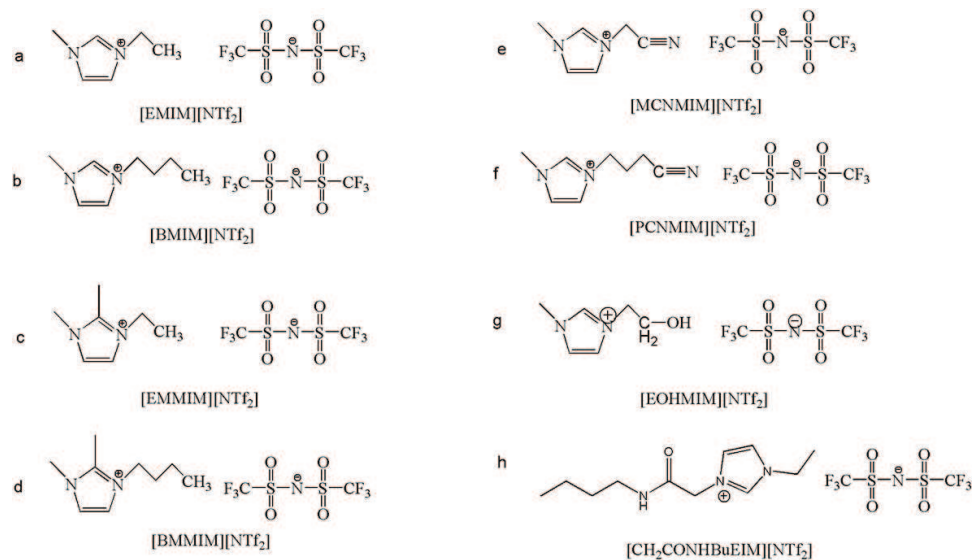

Figure 4. The structures of the (a) [EMIM][NTf$_2$], (b) [BMIM][NTf$_2$], (c) [EMMIM][NTf$_2$], (d) [BMMIM][NTf$_2$], (e) [MCNMIM][NTf$_2$], (f) [PCNMIM][NTf$_2$], (g) [EOHMIM][NTf$_2$], and (h) [CH$_2$CONHBuEIM][NTf$_2$].

The density, dynamic viscosity, and electrical conductivity of the four FILs are listed in **Tables 3–5** [23–25].

The temperature dependences on the density of the FILs [MCNMIM][NTf$_2$], [PCNMIM][NTf$_2$], [EOHMIM][NTf$_2$], and [CH$_2$CONHBuEIM][NTf$_2$] are plotted in **Figure 5**.

In order to compare the influences of methylene and functional group on the properties of ILs, the values of density, dynamic viscosity, and electrical conductivity for ILs are listed in **Table 6** at 298.15 K. The ILs are [EMIM][NTf$_2$], [BMIM][NTf$_2$], [EMMIM][NTf$_2$], [BMMIM][NTf$_2$], [MCNMIM][NTf$_2$], [PCNMIM][NTf$_2$], [EOHMIM][NTf$_2$], and [CH$_2$CONHBuEIM][NTf$_2$], respectively.

	[MCNMIM] [NTf₂]	[PCNMIM] [NTf₂]	[EOHMIM] [NTf₂]	[CH₂CONHBuEIM] [NTf₂]
283.15	1.6259	1.5290	1.5886	1.4310
288.15	1.6205	1.5239	1.5836	1.4270
293.15	1.6150	1.5191	1.5786	1.4227
298.15	1.6097	1.5143	1.5737	1.4180
303.15	1.6046	1.5097	1.5688	1.4135
308.15	1.5996	1.5051	1.5639	1.4090
313.15	1.5946	1.5006	1.5591	1.4044
318.15	1.5898	1.4961	1.5542	1.3997
323.15	1.5848	1.4916	1.5494	1.3954
328.15	1.5799	1.4870	1.5446	1.3910
333.15	1.5751	1.4826	1.5398	1.3867
338.15	1.5702	1.4781	1.5350	1.3823
343.15	1.5654	1.4737	1.5302	
348.15	1.5606	1.4692	1.5255	
353.15	1.5558	1.4648	1.5207	

Table 3. Experimental values of density, ρ/kg·m⁻³, of [MCNMIM][NTf₂], [PCNMIM][NTf₂], [EOHMIM][NTf₂], and [CH₂CONHBuEIM][NTf₂] from 283.15 to 353.15 K at atmosphere pressure.

	[MCNMIM] [NTf₂]	[PCNMIM] [NTf₂]	[EOHMIM] [NTf₂]	[CH₂CONHBuEIM] [NTf₂]
283.15	1140	612.68	213.4	
288.15	708.6	419.66	153.7	
293.15	463.4	303.31	114.1	
298.15	315.5	222.35	86.89	777.5
303.15	222.8	166.86	67.66	517.3
308.15	162.4	131.14	53.88	359.0
313.15	121.7	99.090	43.52	255.2
318.15	93.56	78.438	35.85	187.9
323.15	73.61	63.791	29.83	138.9
328.15	58.99	55.023	25.20	106.0
333.15	47.93	44.728	21.52	82.1
338.15	39.70	37.515	18.46	64.4
343.15	33.27	29.223	16.08	53.3
348.15	28.11	26.418	14.06	43.5
353.15	24.06	23.573	12.44	35.8

Table 4. Experimental values of dynamic viscosity, η/mPa·s, of [MCNMIM][NTf₂], [PCNMIM][NTf₂], [EOHMIM][NTf₂], and [CH₂CONHBuEIM][NTf₂] from 283.15 to 353.15 K at atmosphere pressure.

|	[MCNMIM] [NTf$_2$]	[PCNMIM] [NTf$_2$]	[EOHMIM] [NTf$_2$]	[CH$_2$CONHBuEIM] [NTf$_2$]
283.15	0.283		1.319	0.0606
288.15	0.439	0.612	1.794	0.0985
293.15	0.648	0.841	2.37	0.1527
298.15	0.919	1.125	3.05	0.233
303.15	1.294	1.473	3.87	0.332
308.15	1.727	1.874	4.81	0.467
313.15	2.25	2.33	5.89	0.639
318.15	2.85	2.88	7.04	0.854
323.15	3.60	3.49	8.30	1.106
328.15	4.41	4.17	9.67	1.414
333.15	5.36	4.94	11.12	1.774
338.15	6.44	5.78	12.77	2.19
343.15	7.56	6.66	14.47	
348.15	8.78	7.60	16.26	
353.15	10.12		18.15	

Table 5. Experimental values of electrical conductivity, σ/mS·cm^{-1}, of [MCNMIM][NTf$_2$], [PCNMIM][NTf$_2$], [EOHMIM] [NTf$_2$], and [CH$_2$CONHBuEIM][NTf$_2$] from 283.15 to 353.15 K at atmosphere pressure.
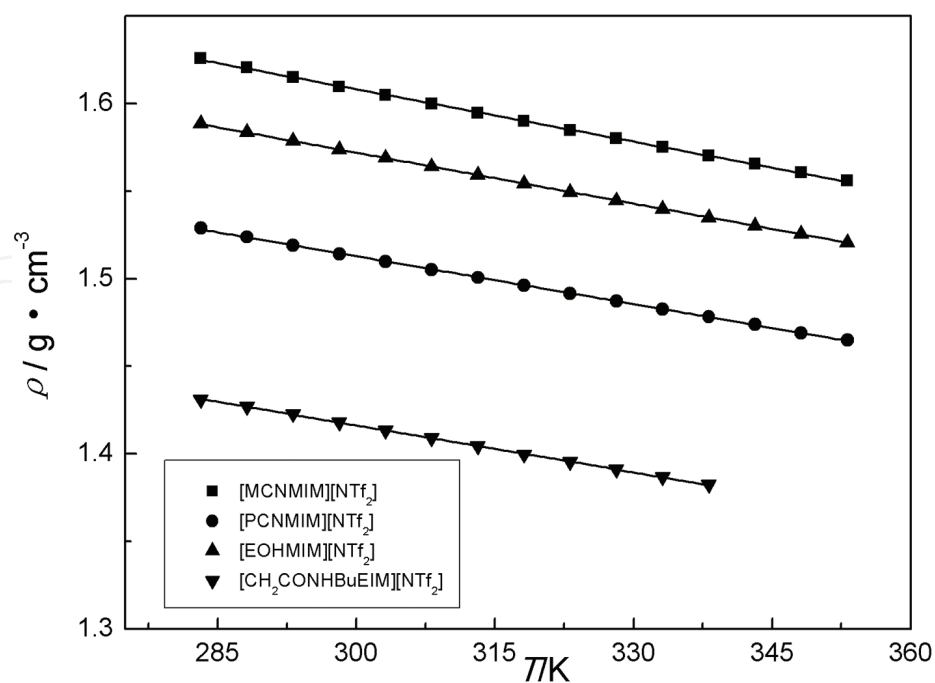
Figure 5. Density vs. temperature plots for FILs [MCNMIM][NTf$_2$], [PCNMIM][NTf$_2$], [EOHMIM][NTf$_2$], and [CH$_2$CON HBuEIM][NTf$_2$].

	MW g mol^{-1}	V cm^3 mol^{-1}	ρ kg m^{-3}	η mPa s	σ mS cm^{-1}
[EMIM][NTf$_2$]	391.31	257.75	1.5182[a]	32.0[a]	8.96[a]
[BMIM][NTf$_2$]	419.36	291.91	1.4366[a]	51.7[a]	3.98[a]
[EMMIM][NTf$_2$]	405.33	271.48	1.4931[a]	72.2[a]	3.89[a]
[BMMIM][NTf$_2$]	433.38	304.70	1.4224[a]	101.6[a]	2.12[a]
[MCNMIM][NTf$_2$]	402.29	249.92	1.6097[b]	315.5[b]	0.919[b]
[PCNMIM][NTf$_2$]	430.34	284.18	1.5143[c]	222.35[c]	1.125[c]
[EOHMIM][NTf$_2$]	407.30	258.8	1.5737	86.89	3.05
[CH$_2$CONHBuEIM][NTf$_2$]	490.47	345.89	1.4180	777.5	0.233

Table 6. Comparison of density, ρ, dynamic viscosity, η, and electrical conductivity, σ, of [EMIM][NTf$_2$], [BMIM][NTf$_2$], [EMMIM][NTf$_2$], [BMMIM][NTf$_2$], [MCNMIM][NTf$_2$], [PCNMIM][NTf$_2$], [EOHMIM][NTf$_2$], and [CH$_2$CONHBuEIM][NTf$_2$] at 298.15 K at atmosphere pressure.

From **Table 6**, based on the same anion, at 298.15 K, the density follows the order of ILs [CH$_2$CONHBuEIM][NTf$_2$] < [BMMIM][NTf$_2$] < [BMIM][NTf$_2$] < [EMMIM][NTf$_2$] < [PCNMIM][NTf$_2$] < [EMIM][NTf$_2$] < [EOHMIM][NTf$_2$] < [MCNMIM][NTf$_2$].

The dynamic viscosity follows the order of ILs [EMIM][NTf$_2$] < [BMIM][NTf$_2$] < [EMMIM][NTf$_2$] < [EOHMIM][NTf$_2$] < [BMMIM][NTf$_2$] < [PCNMIM][NTf$_2$] < [MCNMIM][NTf$_2$] < [CH$_2$CONHBuEIM][NTf$_2$].

The electrical conductivity follows the order of ILs [CH$_2$CONHBuEIM][NTf$_2$] < [MCNMIM][NTf$_2$] < [PCNMIM][NTf$_2$] < [BMMIM][NTf$_2$] < [EOHMIM][NTf$_2$] < [EMMIM][NTf$_2$] < [BMIM][NTf$_2$] < [EMIM][NTf$_2$].

As shown in **Table 6**, the three series ILs have exhibited the same tendency for density after the introduction of methylene on the alkyl side chain. Usually, for dynamic viscosity and electrical conductivity, the introduction of methylene leads to the dynamic viscosity increase and electrical conductivity decrease, such as [EMIM][NTf$_2$] and [BMIM][NTf$_2$]; [EMMIM][NTf$_2$] and [BMMIM][NTf$_2$]. However, for the FILs, the values exhibited the contrary tendency with the traditional ILs. The dynamic viscosity values of FIL [PCNMIM][NTf$_2$] are lower than FIL [MCNMIM][NTf$_2$] and the electrical conductivity values of FIL [PCNMIM][NTf$_2$] are higher than FIL [MCNMIM][NTf$_2$] in the temperature range. The abnormal results have been also discovered for traditional pyridinium-type ILs from our group (see here). For the pyridinium-type ILs, the electrical conductivity values increase when the methyl group is introduced on position 4. The dynamic viscosity values decrease when the methyl group is introduced on position 4. We believed that the electron-withdrawing and electron-donating groups play the important role to the effect of the properties. −CN is the electron-withdrawing group, −CH$_2$− and −CH$_3$ are the electron-donating group. For the two series ILs, the presence of the −CN and −CH$_3$ leads to the cations that have the relatively symmetry structure after the introduction of −CH$_2$−. Then, the cation and anion have the relatively far away and the force of them becomes weak. So, these two types of ILs exhibited the high fluidity after the introduction of −CH$_2$−.

As indicated in **Table 6**, the density and dynamic viscosity of the FILs are higher than the nonfunctional ILs, and the electrical conductivity is lower than the nonfunctional ILs after the introduction of the −CN or −CH_2OH functional group on the imidazolium ring, this result leads to the increasing of Van der Waals force between the cation and the anion relative to the nonfunctional ILs. The order of the effect of the group to the thermodynamic properties is: −CN > −CH_2OH > −CH_3.

According to Eqs. (1)–(4), the calculated values of the thermal expansion coefficient molecular volume, standard molar entropy, and lattice energy are calculated and listed in **Table 7**, respectively.

Property	[MCNMIM] [NTf$_2$]	[PCNMIM] [NTf$_2$]	[EOHMIM] [NTf$_2$]	[CH$_2$CONHBuEIM] [NTf$_2$]
MW/(g mol^{-1})	402.29	430.34	407.30	490.47
V/(nm^3)	0.4151	0.4721	0.4299	0.5746
$10^4 \alpha$/(K^{-1})	6.26	6.09	6.23	6.36
V_m/(cm^{-3} mol^{-1})	249.9	284.18	258.8	345.89
S^0/(J K^{-1} mol^{-1})	547.0	617.9	565.4	745.7
U_{pot}/(kJ mol^{-1})	418	405	414	613

Table 7. Calculated values of thermodynamic properties of FILs [MCNMIM][NTf$_2$], [PCNMIM][NTf$_2$], [EOHMIM] [NTf$_2$], and [CH$_2$CONHBuEIM][NTf$_2$] at 288.15–338.15 K under atmospheric pressure.

From **Table 7**, the contribution of the methylene to the molecular volume is 0.0285 nm^3 for the cyano-type FILs [MCNMIM][NTf$_2$] and [PCNMIM][NTf$_2$]. The value is in good agreement with the reported values of 0.0280 nm^3 for ILs [C$_n$py][NTf$_2$] [4, 26], 0.0282 nm^3 for [C$_n$mim] [NTf$_2$], 0.0277 nm^3 for [C$_n$3mpy][NTf$_2$] (n =3, 4, 6) [27], and 0.0289 nm^3 for [C$_n$4mpy][NTf$_2$] (n =2, 4, 6) [27] at 298.15 K. The lattice energies of the FILs are much lower than traditional salts, such as $U_{POT, CsI}$ = 613 kJ mol^{-1} [28]. Usually, the ILs exhibit the low lattice energy [4, 23–27]. And it is the reason that the ILs having the relatively low melting temperature can exist in the liquid state at room temperature.

Usually, the Vogel-Fulcher-Tammann (VFT) is used for the fitting of temperature dependence on dynamic viscosity. The temperature dependences on dynamic viscosity of the FILs [MCNMIM][NTf$_2$], [PCNMIM][NTf$_2$], [EOHMIM][NTf$_2$], and [CH$_2$CONHBuEIM][NTf$_2$] are plotted in **Figure 6**.

The best fitted values of η_0, B, T_0, and the correlation coefficient, R, are listed in **Table 8** from the empirical Eq. (11). From **Table 8**, the obtained correlation coefficient values, R, are better than 0.9999. The results indicate that the experimental dynamic viscosity of the FILs [MCNMIM][NTf$_2$], [PCNMIM][NTf$_2$], [EOHMIM][NTf$_2$], and [CH$_2$CONHBuEIM][NTf$_2$] can be fitted by the VFT equation.

According to Eq. (12), the 1000/T dependence of ln η was plotted for four FILs [MCNMIM] [NTf$_2$], [PCNMIM][NTf$_2$], [EOHMIM][NTf$_2$], and [CH$_2$CONHBuEIM][NTf$_2$] (see **Figure 7**).
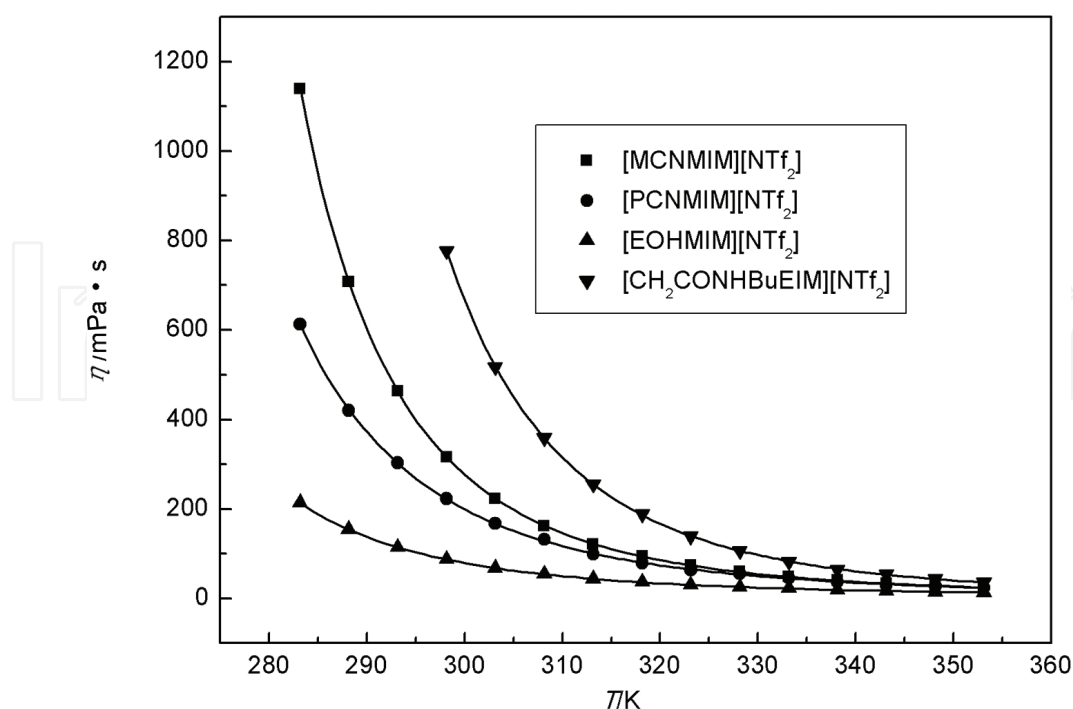
Figure 6. Dynamic viscosity vs. temperature plots for FILs [MCNMIM][NTf$_2$], [PCNMIM][NTf$_2$], [EOHMIM][NTf$_2$], and [CH$_2$CONHBuEIM][NTf$_2$].

Property	[MCNMIM] [NTf$_2$]	[PCNMIM] [NTf$_2$]	[EOHMIM] [NTf$_2$]	[CH$_2$CONHBuEIM] [NTf$_2$]
η_0/(mPa s)	0.2166	0.1600	0.2144	0.0820
B/K	728.8	882.1	692.3	990.9
$10^3 E_\eta$/eV	62.9	76.1	59.7	85.5
T_0/K	198.1	176.2	182.9	189.9
R	0.99999	0.99989	0.99999	0.99998

Table 8. Fitted parameter values of η_0, B, T_0, and correlation coefficient, R, and E_η.

The 1000/T dependences on ln η of the four FILs [MCNMIM][NTf$_2$], [PCNMIM][NTf$_2$], [EOHMIM][NTf$_2$], and [CH$_2$CONHBuEIM][NTf$_2$] are also fitted in the temperature range (**Figure 7**). The values of the correlation coefficient, R, are 0.9878, 0.9937, 0.9926, and 0.9943, respectively. The values are obvious lower than the correlation coefficient values, R = 0.99999, 0.99989, 0.99999, and 0.99998, which obtained according to the VFT equation. So, the same result indicated that the dynamic viscosity values of [MCNMIM][NTf2], [PCNMIM][NTf2], [EOHMIM][NTf2], and [CH2CONHBuEIM][NTf2] cannot be fitted according to the Arrhenius Eq. (12). From **Figure 7**, it can be obviously observed that the measurement points lie far away from the fitted straight lines.

According to Eq. (13), the activation energies of dynamic viscosity for the FILs [MCNMIM][NTf$_2$], [PCNMIM][NTf$_2$], [EOHMIM][NTf$_2$], and [CH$_2$CONHBuEIM][NTf$_2$] were calculated and are listed in **Table 8**.

From **Table 5**, the temperature dependences on electrical conductivity of the FILs [MCNMIM][NTf$_2$], [PCNMIM][NTf$_2$], [EOHMIM][NTf$_2$], and [CH$_2$CONHBuEIM][NTf$_2$] are plotted in **Figure 8**.
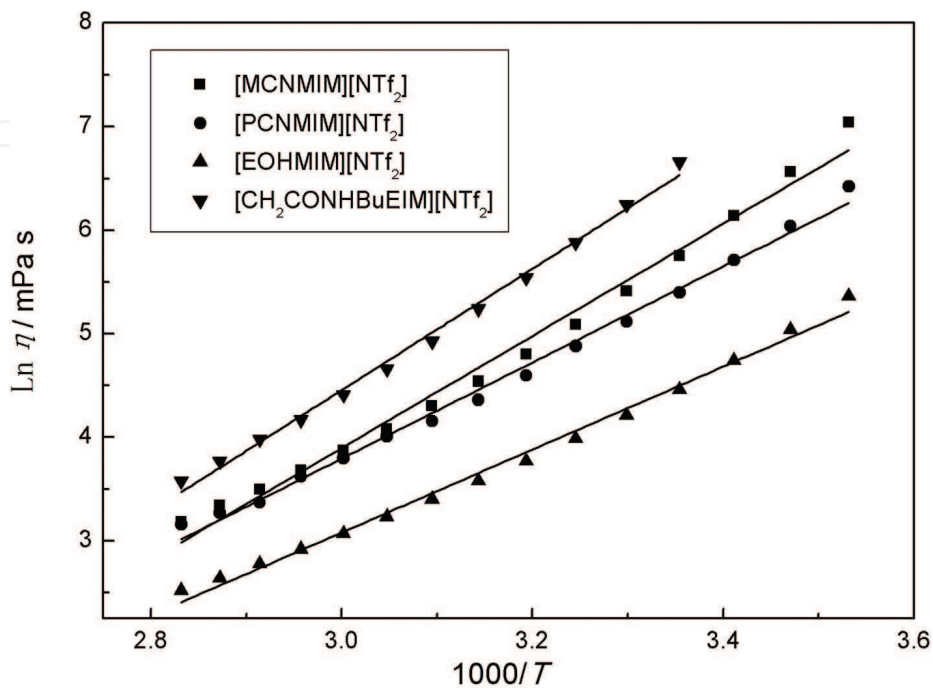

Figure 7. Plot of lnη vs. 1000/T for FILs [MCNMIM][NTf$_2$], [PCNMIM][NTf$_2$], [EOHMIM][NTf$_2$], and [CH$_2$CONHBuEIM][NTf$_2$].
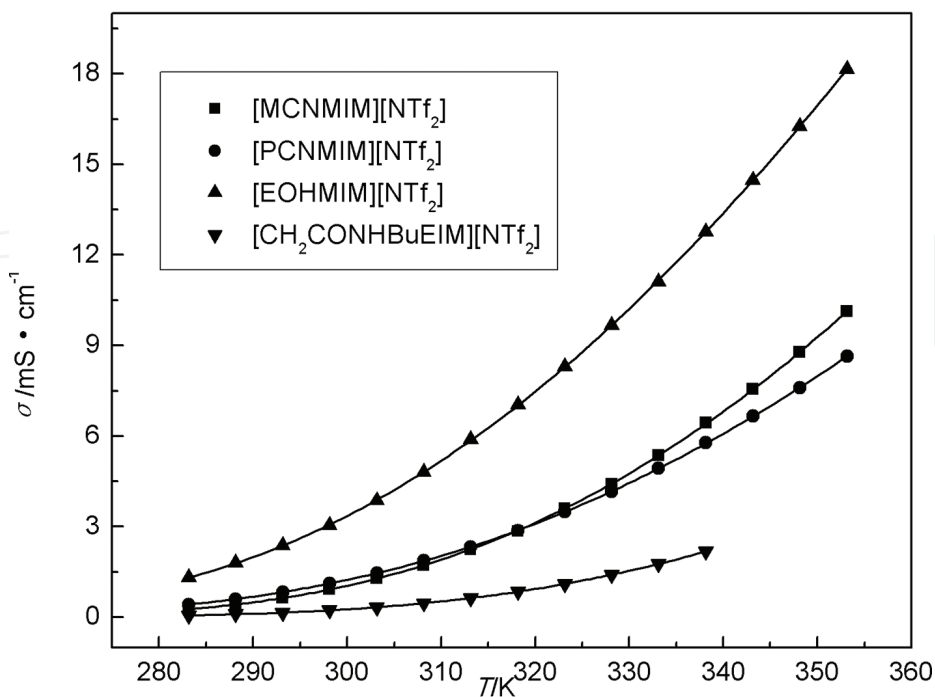

Figure 8. Electrical conductivity vs. temperature plots for FILs [MCNMIM][NTf$_2$], [PCNMIM][NTf$_2$], [EOHMIM][NTf$_2$], and [CH$_2$CONHBuEIM][NTf$_2$].

The best fitted values of σ_0, B, T_0, and the correlation coefficient, R, are listed in **Table 9** from the empirical Eq. (14). From **Table 9**, the obtained correlation coefficient, R, is better than 0.9999. The results indicate that the measurement electrical conductivity of the FILs [MCNMIM][NTf$_2$], [PCNMIM][NTf$_2$], [EOHMIM][NTf$_2$], and [CH$_2$CONHBuEIM][NTf$_2$] can be fitted by the VFT equation.

According to Eq. (15), the $1000/T$ dependence on $\ln \sigma$ was plotted of four FILs [MCNMIM][NTf$_2$], [PCNMIM][NTf$_2$], [EOHMIM][NTf$_2$], and [CH$_2$CONHBuEIM][NTf$_2$] (see **Figure 9**).

Property	[MCNMIM] [NTf$_2$]	[PCNMIM] [NTf$_2$]	[EOHMIM] [NTf$_2$]	[CH$_2$CONHBuEIM] [NTf$_2$]
$\sigma_0/(S\cdot cm^{-1})$	0.64	0.49	0.56	0.82
B/K	621.3	661.8	551.9	860.5
$10^3 E_\sigma/eV$	53.6	57.1	47.6	74.3
T_0/K	203.0	189.3	192.0	192.9
R	0.99997	0.99997	0.99998	0.99999

Table 9. Fitted parameter values of σ_0, B, T_0, correlation coefficient, R and E_σ.
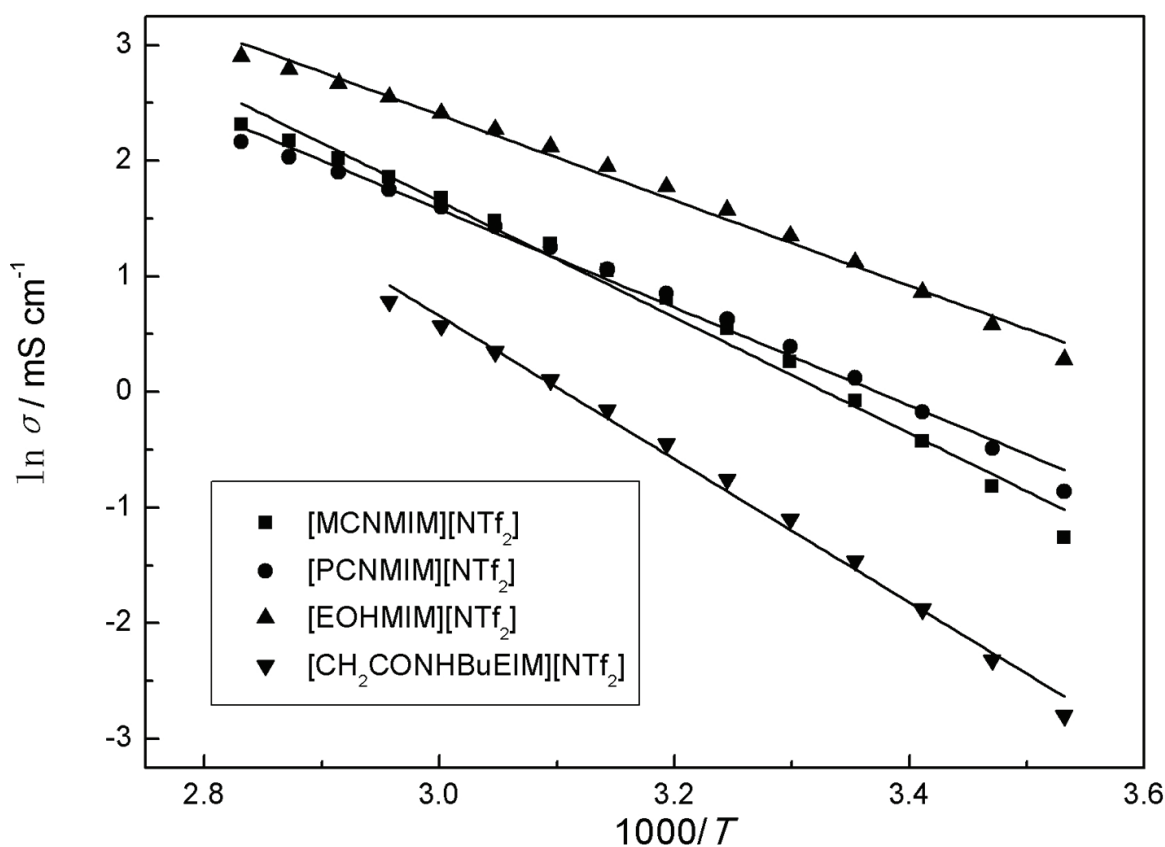

Figure 9. Plot of $\ln \sigma$ and $\ln\sigma$ vs. $1000/T$ for FILs [MCNMIM][NTf$_2$], [PCNMIM][NTf$_2$], [EOHMIM][NTf$_2$], and [CH$_2$CONHBuEIM][NTf$_2$].

In **Figure 9**, the $1000/T$ dependences on $\ln \sigma$ of the four FILs [MCNMIM][NTf$_2$], [PCNMIM] [NTf$_2$], [EOHMIM][NTf$_2$], and [CH$_2$CONHBuEIM][NTf$_2$] are fitted in the temperature range. The values of the correlation coefficient, R, are 0.9878, 0.9908, 0.9905, and, 0.9930, respectively. The same results can be obtained that the values are much lower than the correlation coefficient values, $R = 0.99997$, 0.99998, 0.99998, and 0.99999, which obtained by the VFT equation (see **Table 9**). So, the measurement electrical conductivity of [MCNMIM][NTf$_2$], [PCNMIM] [NTf$_2$], [EOHMIM][NTf$_2$], and [CH$_2$CONHBuEIM][NTf$_2$] does not well follow the Arrhenius Eq. (15). From **Figure 9**, it can be obviously seen that the measurement points lie far away from the fitted straight lines.

The activation energies of electrical conductivity for four FILs [MCNMIM][NTf$_2$], [PCNMIM] [NTf$_2$], [EOHMIM][NTf$_2$], and [CH$_2$CONHBuEIM][NTf$_2$] were also calculated by Eq. (16) and are listed in **Table 9**.

At 298.15 K, the Walden's product (in [S·cm^2·mol^{-1}][mP·s]) for the four FILs [MCNMIM][NTf$_2$], [PCNMIM][NTf$_2$], [EOHMIM][NTf$_2$], and [CH$_2$CONHBuEIM][NTf$_2$] can be determined according to Eq. (17), and the values are 73, 71, 69, and 63, respectively.

According to Eq. (17), the $\log \Lambda$ dependences on $\log \eta^{-1}$ are illustrated in **Figure 10** for the four FILs [MCNMIM][NTf$_2$], [PCNMIM][NTf$_2$], [EOHMIM][NTf$_2$], and [CH$_2$CONHBuEIM][NTf$_2$] from 283.15 to 353.15 K.
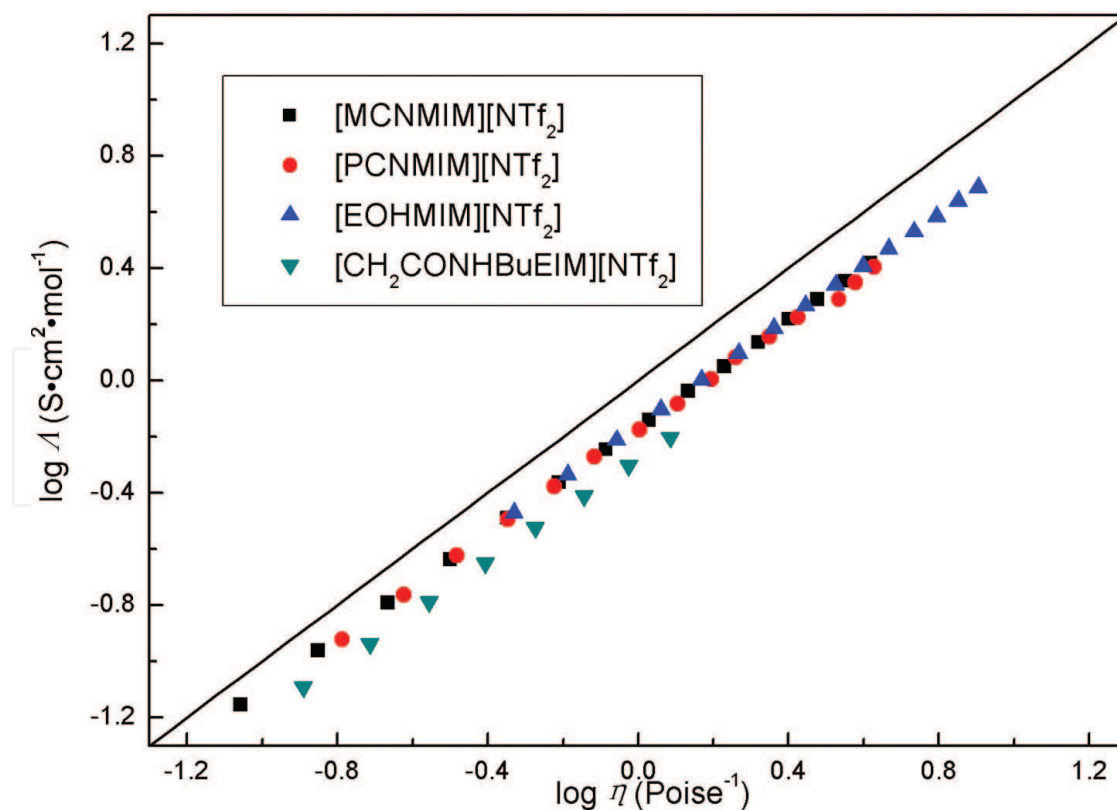

Figure 10. Plot of lgΛ vs. lgη^{-1} for the four FILs [MCNMIM][NTf$_2$], [PCNMIM][NTf$_2$], [EOHMIM][NTf$_2$], and [CH$_2$CONHBuEIM][NTf$_2$] from 283.15 to 353.15 K. The solid straight line is the ideal line for aqueous KCl solutions.

Usually, the Walden rule can be used for the presentation of the independent ions of the liquid. If the Walden points close to the ideal line, the liquid can be considered as a relative ideal liquid. The ideal line position was determined according to the aqueous KCl solution at high dilution. As an ideal line, the slop of the ideal line should be unity and not have any interaction of the ions [10, 29, 30]. In **Figure 10**, it can be seen that the approximately straight lines can be obtained according to the experimental points. The results indicate that the FILs [MCNMIM][NTf$_2$], [PCNMIM][NTf$_2$], [EOHMIM][NTf$_2$], and [CH$_2$CONHBuEIM][NTf$_2$] follow the Walden rule to some extent. The slopes of the lines for the four FILs [MCNMIM][NTf$_2$], [PCNMIM][NTf$_2$], [EOHMIM][NTf$_2$], and [CH$_2$CONHBuEIM][NTf$_2$] are 0.941, 0.927, 0.939, and 0.913, respectively. The lines for the two FILs below are close to the ideal KCl line, as shown in **Figure 10**. Most of the reported traditional ILs [9, 10, 29, 31] and our previous studied ILs [24–27, 32, 33] have the same trend. From the result, the FILs [MCNMIM][NTf$_2$], [PCNMIM][NTf$_2$], [EOHMIM][NTf$_2$], and [CH$_2$CONHBuEIM][NTf$_2$] can be named "subionic" [34].

Conclusion

The density, dynamic viscosity, and electrical conductivity of the FILs [MCNMIM][NTf$_2$], [PCNMIM][NTf$_2$], [EOHMIM][NTf$_2$], and [CH$_2$CONHBuEIM][NTf$_2$] were measured at the temperature from 283 to 353 K. The others thermodynamic properties of the FILs, like thermal expansion coefficient, molecular volume, standard molar entropy, and lattice energy, were estimated according to the classical empirical equations. The introduction of the methylene group on the −CN (electron-withdrawing group) type series FILs leads to a different change in the dynamic viscosity, and electrical conductivity with the traditional ILs. The dynamic viscosity values of FIL [PCNMIM][NTf$_2$] are lower than FIL [MCNMIM][NTf$_2$] and the electrical conductivity values of FIL [PCNMIM][NTf$_2$] are higher than FIL [MCNMIM][NTf$_2$] in the temperature range. The temperature dependences on the dynamic viscosity and electrical conductivity values of the ILs can be satisfactorily fitted by the VFT equation. However, the experimental values do not follow the Arrhenius behavior described by the Arrhenius equation.

8. Density, dynamic viscosity, and electrical conductivity of pyridinium-based hydrophobic ionic liquids

Actually, most of the studied ILs are hydrophilic-type ILs. The hydrophobic ILs have been paid much more attention in many fields as a special functional ILs. The bis(trifluoromethylsulfonyl)imide [NTf$_2$]$^-$ as an air- and water-stable anion has been applied in many fields [35–37]. These types of anion ILs have exhibited a relatively wide liquid range, higher electrical conductivity, and thermal stability than the hydrophilic-type ILs. However, the study of thermodynamic properties of the [NTf$_2$]-type ILs mainly focuses on the imidazolium-type cation ILs [38–40]. The study of the pyridinium type cation-based ILs is still not

enough [41]. The systematical research on the properties including density, dynamic viscosity, and electrical conductivity is still scarce which can provide the well information of the suitable IL for a specific purpose.

In this section, the basic physicochemical properties of three serious Ils N-alkylpyridinium bis(trifluoromethylsulfonyl)imide $\{[C_npy][NTf_2]$ $(n = 2, 3, 4, 5, 6)\}$, N-alkyl-3-methylpyridinium bis(trifluoromethyl-sulfonyl)imide $\{[C_n3Mpy][NTf_2]$ $(n = 3, 4, 6)\}$, and N-alkyl-4-methylpyridinium bis(trifluoromethylsulfonyl)imide $\{[C_n4Mpy][NTf_2]$ $(n = 2, 4, 6)\}$ were discussed. The methyl group was introduced on positions 3 and 4 of the pyridinium ring, respectively. The basic physicochemical properties, including density, dynamic viscosity, and electrical conductivity, were measured by the traditional methods. The other physicochemical properties, including molecular volume, standard molar entropy, lattice energy, were estimated in terms of empirical and semiempirical equations on the basis of the experimental value. The effect of the methylene and methyl groups on the properties is discussed at 298.15 K.

The structures of ILs $[C_npy][NTf_2]$ $(n = 2, 3, 4, 5, 6)$, $[C_n3Mpy][NTf_2]$ $(n = 3, 4, 6)$, and $[C_n4Mpy]$ $[NTf_2]$ $(n = 2, 4, 6)$ are shown in **Figure 11**.
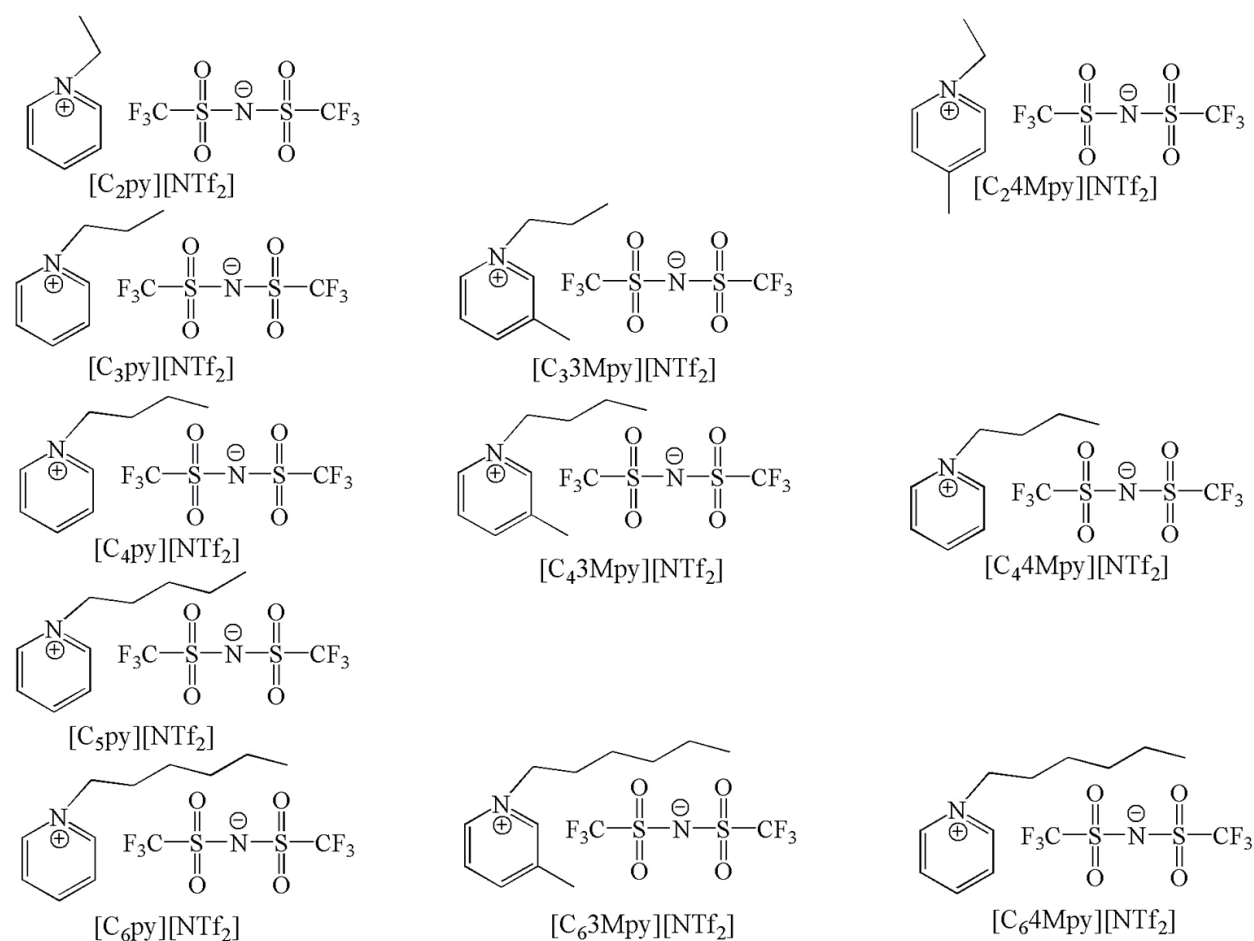

Figure 11. The structure of ILs $[C_npy][NTf_2]$ $(n = 2, 3, 4, 5, 6)$, $[C_n3Mpy][NTf_2]$ $(n = 3, 4, 6)$, and $[C_n4Mpy][NTf_2]$ $(n = 2, 4, 6)$.

8.1. N-Alkyl type pyridinium type ionic liquids

The results of the density, surface tension, dynamic viscosity, and electrical conductivity of the ILs $[C_npy][NTf_2]$ (n = 2, 3, 4, 5, 6) are listed in **Tables 10–13** [4, 31, 33].

	$[C_2py][NTf_2]$	$[C_3py][NTf_2]$	$[C_4py][NTf_2]$	$[C_5py][NTf_2]$	$[C_6py][NTf_2]$
283.15				1.4331	1.4008
288.15	1.5457			1.4296	1.3966
293.15	1.5414			1.4259	1.3923
298.15	1.5375		1.4547	1.4214	1.3877
303.15	1.5332		1.4506	1.4169	1.3831
308.15	1.5291	1.4845	1.4462	1.4128	1.3789
313.15	1.5249	1.4800	1.4417	1.4083	1.3744
318.15	1.5205	1.4757	1.4372	1.4038	1.3699
323.15	1.5164	1.4710	1.4332	1.3989	1.3655
328.15	1.5122	1.4667	1.4291	1.3942	1.3615
333.15	1.5078	1.4623	1.4245	1.3893	1.3569
338.15	1.5037	1.4574	1.4205	1.3851	1.3525

Table 10. Experimental values of density of ILs $[C_npy][NTf_2]$ (n = 2, 3, 4, 5, 6).

	$[C_2py][NTf_2]$	$[C_3py][NTf_2]$	$[C_4py][NTf_2]$	$[C_5py][NTf_2]$	$[C_6py][NTf_2]$
283.15				33.1	32.5
288.15	37.7			32.8	32.2
293.15	37.6			32.7	32.0
298.15	37.4		33.4	32.5	31.7
303.15	37.1		33.2	32.2	31.6
308.15	36.9		32.9	32.0	31.4
313.15	36.7		32.8	31.8	31.2
318.15	36.6		32.4	31.5	31.0
323.15	36.4		32.1	31.3	30.8
328.15	36.1		32.0	31.1	30.6
333.15	35.9		31.8	30.8	30.3
338.15	35.6		31.5	30.5	30.1

Table 11. Experimental values of surface tension of ILs $[C_npy][NTf_2]$ (n = 2, 3, 4, 5, 6).

	$[C_2py][NTf_2]$	$[C_3py][NTf_2]$	$[C_4py][NTf_2]$	$[C_5py][NTf_2]$	$[C_6py][NTf_2]$
298.15	39.4		58.3	71.9	84.5
303.15	32.5		46.7	57.1	66.4
308.15	27.1	33.0	38.0	45.6	53.2
313.15	23.2	27.6	31.4	37.2	43.1
318.15	20.0	23.3	26.4	30.6	35.2
323.15	17.3	19.8	22.4	25.6	29.1
328.15	15.2	17.1	19.2	21.7	24.5
333.15	13.5	14.9	16.6	18.4	20.9
338.15	11.9	13.5	14.4	15.8	17.9

Table 12. Experimental values of dynamic viscosity of ILs $[C_npy][NTf_2]$ (n = 2, 3, 4, 5, 6).

	$[C_2py][NTf_2]$	$[C_3py][NTf_2]$	$[C_4py][NTf_2]$	$[C_5py][NTf_2]$	$[C_6py][NTf_2]$
283.15			1.67	1.04	0.76
288.15			1.91	1.37	1.00
293.15	5.01		2.50	1.77	1.30
298.15	5.99		3.21	2.22	1.66
303.15	7.06		3.95	2.75	2.08
308.15	8.24		4.73	3.36	2.57
313.15	9.53	7.19	5.63	4.03	3.11
318.15	10.90	8.30	6.70	4.81	3.87
323.15	12.33	9.55	7.79	5.63	4.46
328.15	14.28	10.83	8.96	6.53	5.38
333.15	16.09	12.23	10.19	7.42	6.21
338.15	17.84	13.65	11.47	8.24	7.12

Table 13. Experimental values of electrical conductivity of ILs $[C_npy][NTf_2]$ (n = 2, 3, 4, 5, 6).

From **Tables 10–13**, it can be concluded that the density and electrical conductivity decrease as the alkyl side chain length of the cation increases for the N-alkyl type pyridinium ILs. The dynamic viscosity increases with the extension of the alkyl side chain of the cation for the three series of N-alkyl type pyridinium ILs.

According to Eqs. (1)–(10), the thermodynamic properties are calculated and listed in **Table 14**, respectively.

Property	$[C_2py][NTf_2]$	$[C_4py][NTf_2]$	$[C_5py][NTf_2]$	$[C_6py][NTf_2]$
$10^3 S_a / mJ \cdot K^{-1} \cdot m^{-2}$	41.6	47.9	46.2	41.8
$E_a / mJ \cdot m^{-2}$	49.8	47.7	46.3	44.1
V_m / nm^3	0.4196	0.4754	0.5030	0.5320
$S^0 / J \cdot K^{-1} \cdot mol^{-1}$	552.5	622.1	656.4	692.6
$10^7 k / J \cdot K^{-1}$	1.131	1.590	1.503	1.316
T_c / K	1618	1212	1271	1429
T_b / K	970	727	763	857
$U_{pot} / kJ \cdot mol^{-1}$	417	404	399	393
$V / cm^{-3} \cdot mol^{-1}$	252.6	286.2	302.8	320.2
p	625.0	688.9	723.5	759.9
$\Delta_l^g H_m^0 / kJ \cdot mol^{-1}$	143.8	139.1	140.9	142.9
$10^{24} v / cm^3$	24.80	29.38	30.67	31.77
$\sum v / cm^3$	29.86	35.38	36.92	38.25
$10^2 \sum v / V$	11.82	12.36	12.19	11.95
$10^4 \alpha / K^{-1}$ (exp.)	5.63	5.99	6.30	6.40
$10^4 \alpha / K^{-1}$ (cal.)	5.95	6.22	6.13	6.01

Table 14. Estimated values of physicochemical properties of $[C_n py][NTf_2]$ at 298.15 K.

From **Table 14**, the thermal expansion coefficients are 5.63×10^{-4}, 5.99×10^{-4}, 6.30×10^{-4}, and 6.40×10^{-4} K^{-1} for $[C_2py][NTf_2]$, $[C_4py][NTf_2]$, $[C_5py][NTf_2]$, and $[C_6py][NTf_2]$, respectively. The values are in good agreement in the range of 5×10^{-4} to 7×10^{-4} K^{-1} obtained by Jacquemin et al. [40]. From **Table 14**, compared with the fused salts and organic liquids, for example, $E_a = 146$ $mJ \cdot m^{-2}$ for $NaNO_3$, $E_a = 67$ $mJ \cdot m^{-2}$ for benzene and $E_a = 51.1$ $mJ \cdot m^{-2}$ for octane. The values of surface energy of the samples are close to the organic liquids. This fact shows that the interaction energy between ions in the samples is less than fused salts. The values of the molecular volume are 0.4196 nm^3 for $[C_2py][NTf_2]$, 0.4754 nm^3 for $[C_4py][NTf_2]$, 0.5030 nm^3 for $[C_5py][NTf_2]$, and 0.5320 nm^3 for $[C_6py][NTf_2]$ at 298.15 K. The plotting V_m against the number of the carbons, n, in the alkyl chain of the samples ($[C_n py][NTf_2]$) can be described (see **Figure 4**). The average contribution of the methylene to the molecular volume can be obtained by the slop of the fitting equation. The value is 0.0280 nm^3 at 298.15 K. The value is close to the values of 0.0272 nm^3 for imidazolium-type ILs $[C_n mim][BF_4]$ and 0.0282 nm^3 for imidazolium-type $[C_n mim][NTf_2]$.

The molar masses of cations of the ILs $[C_n py][NTf_2]$ ($n = 2, 4, 5, 6$) are listed in **Table 15**. The plotting V_m against the molar mass of cations of the samples ($[C_n py][NTf_2]$) can be obtained (see **Figure 12**). The intercept of the linear regression can be approximately regarded the volume of the anion, NTf_2^-, the value is 0.2032 nm^3. The volume value of NTf_2^- is much higher than 0.1390 nm^3 for $AlCl_4^-$ [42] and 0.1548 nm^3 $GaCl_4^-$ [43]. The volume values of the cations and the radii are listed in **Table 15**.

	$\rho/\mathrm{g\cdot cm^{-3}}$	$V_m/\mathrm{nm^3}$	M_+	$V_+/\mathrm{nm^3}$	r_+/nm
[C$_2$py][NTf$_2$]	1.5375	0.4196	108.16	0.2164	0.372
[C$_4$py][NTf$_2$]	1.4547	0.4754	136.22	0.2722	0.402
[C$_5$py][NTf$_2$]	1.4214	0.5030	150.24	0.2998	0.415
[C$_6$py][NTf$_2$]	1.3877	0.5320	164.27	0.3288	0.428

Table 15. Estimated volumetric properties of the ILs [C$_n$py][NTf$_2$] n = 2, 4, 5, 6 at 298.15 K.
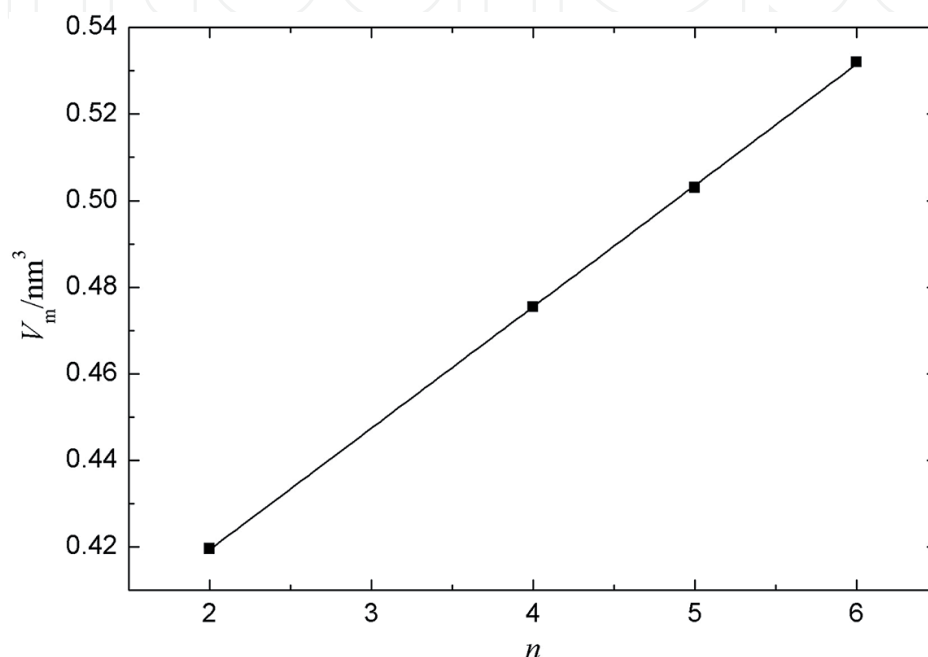
Figure 12. Plot of V_m vs. n at 298.15 K, the correlation coefficient is R = 0.9999 for ILs [C$_n$py][NTf$_2$] (n = 2, 4, 5, 6).

According to Eq. (5), by plotting the $\gamma V_m^{2/3}$ against T, straight lines were obtained (see **Figure 13**). From the plot, the value of empirical constant (k) and critical temperature (T_c) can be obtained according to the fitting equation and the values are listed in **Table 16**. Rebelo et al. [44] have reported that the normal boiling point, T_b, is approximately $0.6T_c$ for ILs. Herein, the normal boiling point, T_b, can be calculated and the values are also listed in **Table 16**. For the majority of organic liquids, $k \approx 2.1 \times 10^{-7}$ J·K^{-1}, but for fused salts, $k = 0.4 \times 10^{-7}$ J·K^{-1} for fused NaCl [7]. It indicated that ILs [C$_n$py][NTf$_2$] (n = 2, 4, 5, 6) have the medium polarity between organic liquids and fused salts in terms of the value of the k.

From **Table 14**, the values of estimation of the thermal expansion coefficient are in good agreement with experimental values. It also can be seen that the estimation values of interstice fractions, $\sum v/V$, are in the range of 11–13% for the ILs [C$_n$py][NTf$_2$] (n = 2, 4, 5, 6). For the majority materials, the volume expansions are in the range of 10–15% from the solid state to liquid state. For the ILs [C$_n$py][NTf$_2$] (n = 2, 4, 5, 6), the values are in good agreement with the reported values. Therefore, the interstice model theory can be used for calculation of the thermal expansion coefficient of pyridinium-based ILs.
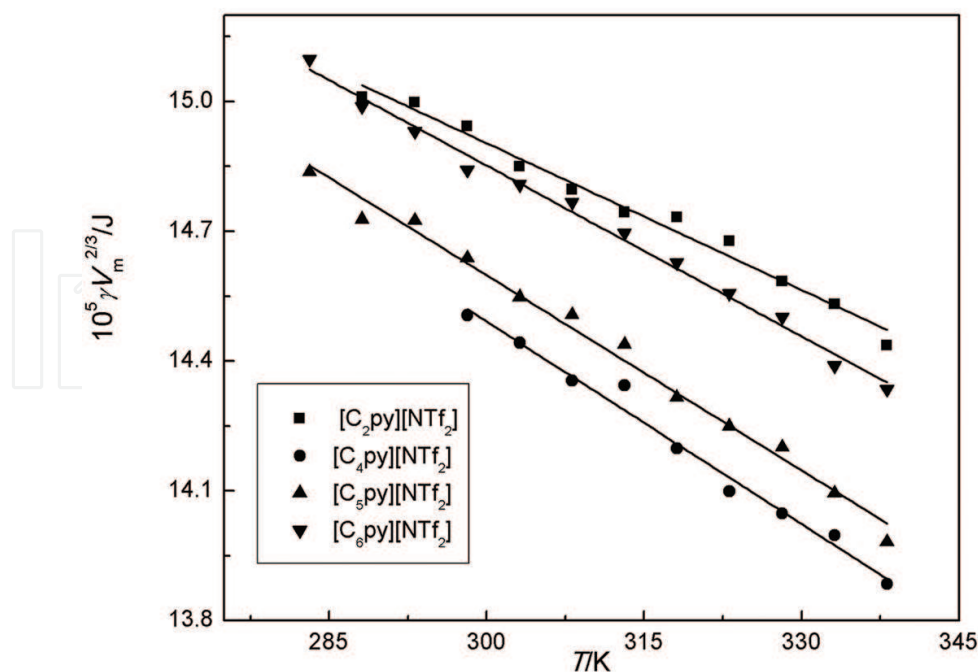
Figure 13. Plot of $\gamma V_m^{2/3}$ vs. T (K) for ILs[$C_n$py][NTf$_2$] (n = 2, 4, 5, 6).

	[C$_2$py][NTf$_2$]	[C$_4$py][NTf$_2$]	[C$_5$py][NTf$_2$]	[C$_6$py][NTf$_2$]
$10^7 K/J \cdot K^{-1}$	1.131	1.559	1.503	1.316
T_b/K	1618	1230	1815	1429
T_c/K	971	738	1089	857

Table 16. The estimated values of k, T_b, and T_c for ILs [C$_n$py][NTf$_2$] n = 2, 4, 5, 6.

According to **Table 12** and Eq. (11), the temperature dependence on dynamic viscosity values of the ILs can also be fitted using the VFT Eq. (11), see **Figure 14**.

The best fitting parameters of η_0, B, T_0, and the corresponding correlation coefficient, R, are listed in **Table 17**. From **Table 17**, the obtained values of the correlation coefficient, R, are 0.9999, which indicates that the VFT equation can be used for fitting the experimental dynamic viscosity.

According to Eq. (13), the activation energies of dynamic viscosity for [C$_n$py][NTf$_2$] (n = 2, 4, 5, 6) were calculated by Eq. (13) and are listed in **Table 17**.

According to Eq. (12), the 1000/T dependence of ln η was plotted for [C$_n$py][NTf$_2$] (n = 2, 3, 4, 5, 6) (see **Figure 15**).

The 1000/T dependences on ln η of the for [C$_n$py][NTf$_2$] (n = 2, 3, 4, 5, 6) were fitted in the temperature range (see **Figure 15**). The values of the correlation coefficient, R, are 0.9976, 0.9965,

0.9977, 0.9984, and 0.9983, respectively. The values are obviously lower than the values (all of the values are 0.9999) which obtained by the empirical VFT equation. So, the measurement dynamic viscosity of $[C_npy][NTf_2]$ (n = 2, 3, 4, 5, 6) does not follow the Arrhenius Eq. (12). From **Figure 15**, it can also be obviously seen that the measurement points lie far away from the fitted straight lines. The FILs $[MCNMIM][NTf_2]$, $[PCNMIM][NTf_2]$, $[EOHMIM]$ $[NTf_2]$, and $[CH_2CONHBuEIM][NTf_2]$ have also exhibited the same result.
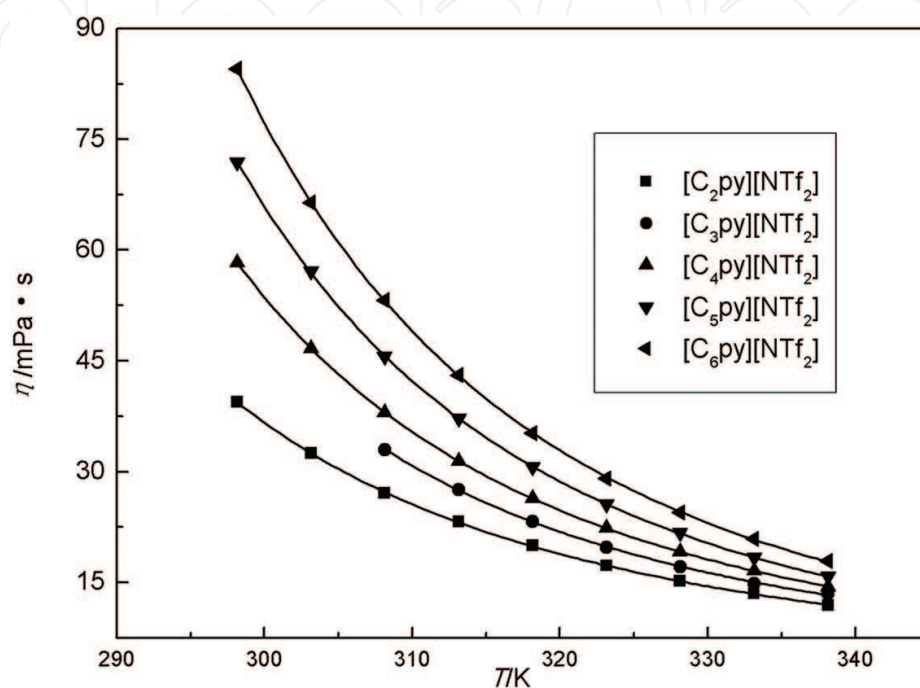
Figure 14. Plot of dynamic viscosity, η, vs. temperature, T, of ILs $[C_npy][NTf_2]$ (n = 2, 3, 4, 5, 6).

Property	$[C_2py][NTf_2]$	$[C_4py][NTf_2]$	$[C_5py][NTf_2]$	$[C_6py][NTf_2]$
$\eta_0/(\text{mPa·s})$	0.3907	0.2021	0.0758	0.0645
B/K	531.7	695.1	966.2	1036.0
$10^3E_\eta/eV$	45.9	60.0	83.4	89.4
T_0/K	182.9	175.4	157.2	153.8
R	0.9999	0.9999	0.9999	0.9999

Table 17. Fitted values of dynamic viscosity of η_0, B, E_η, T_0, and R according to Eqs. (11) and (13).

According to **Table 13** and Eq. (14), the temperature dependences of electrical conductivity values of the ILs can also be fitted using the VFT Eq. (14), see **Figure 16**.

The best-fitting parameters of σ_0, B, T_0, and the corresponding correlation coefficient, R, are listed in **Table 18**. From **Table 18**, the obtained values of the correlation coefficient, R, are 0.9996, which indicates that the VFT equation can be used for fitting the experimental electrical conductivity.
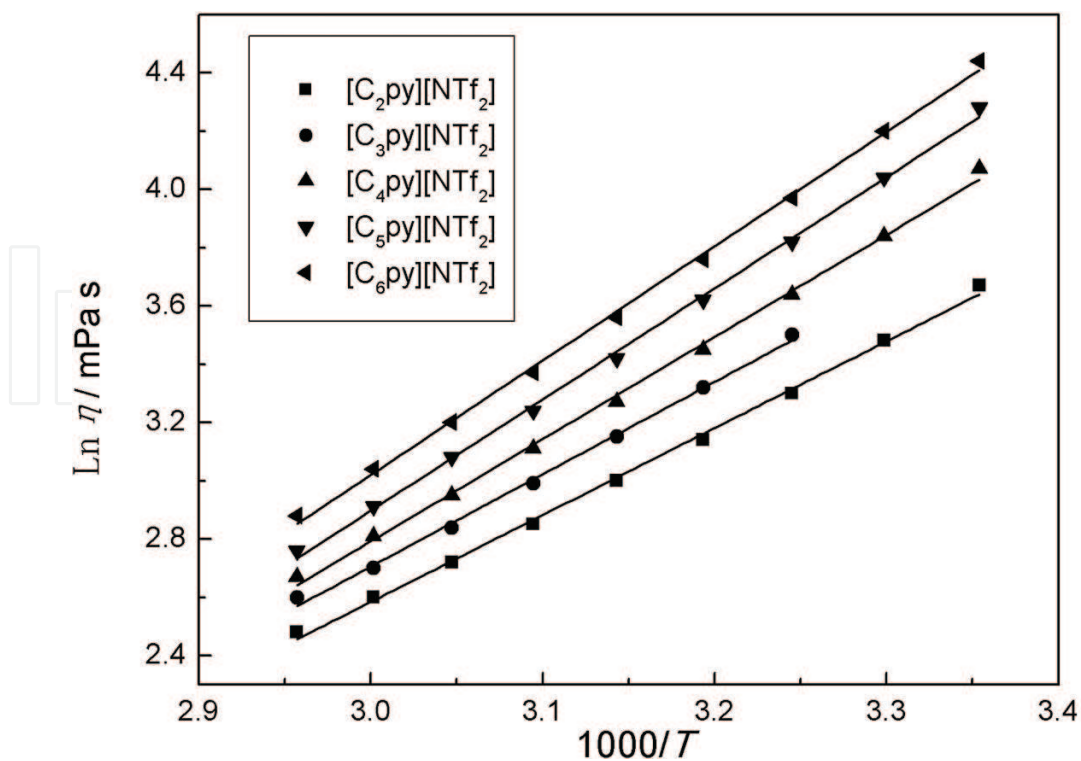
**Figure 15.** Plot of dynamic viscosity, η, vs. temperature, T, of $[C_n py][NTf_2]$ (n = 2, 3, 4, 5, 6).
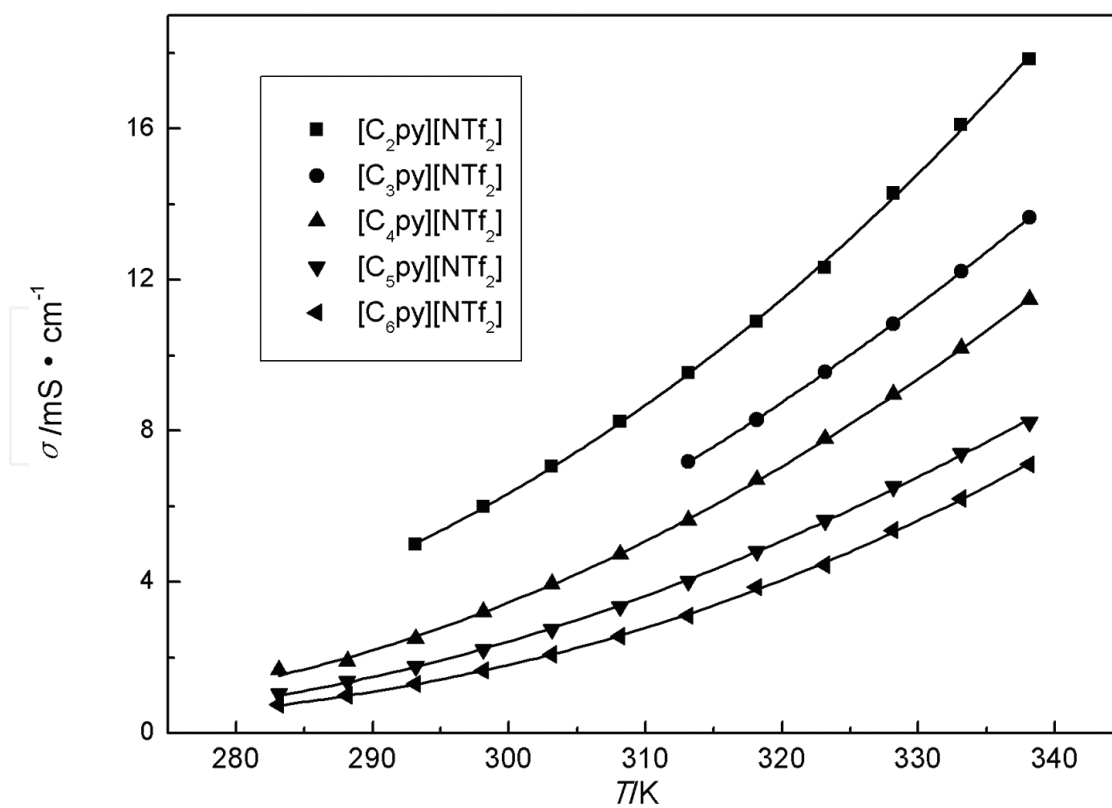
Figure 16. Plot of electrical conductivity, σ, vs. temperature, T, of $[C_n py][NTf_2]$ (n = 2, 3, 4, 5, 6).

Property	[C$_2$py][NTf$_2$]	[C$_4$py][NTf$_2$]	[C$_5$py][NTf$_2$]	[C$_6$py][NTf$_2$]
$\sigma_0/(\text{S}\cdot\text{cm}^{-1})$	2.39	0.47	0.23	0.81
B/K	1067.5	577.7	472.9	803.1
$10^3 E_\sigma/\text{eV}$	92.1	49.9	40.8	69.3
T_0/K	119.9	182.3	196.5	168.4
R	0.9996	0.9996	0.9996	0.9996

Table 18. Fitted values of electrical conductivity of σ_0, B, E_σ, T_0, and R according to Eqs. (**15**) and (**17**).

According to Eq. (16), the activation energies of dynamic viscosity for [C$_n$py][NTf$_2$] ($n = 2, 4, 5, 6$) were calculated by Eq. (16) and are listed in **Table 18**.

According to Eq. (15), the 1000/T dependence on ln σ was also plotted for the [C$_n$py][NTf$_2$] ($n = 2$, 4, 5, 6) (see **Figure 17**).

In **Figure 17**, the 1000/T dependence on ln σ of the [C$_n$py][NTf$_2$] ($n = 2, 3, 4, 5, 6$) was fitted in the temperature range. The values of the correlation coefficient, R, are 0.9990, 0.9990, 0.9939, and 0.9970, respectively. The values are also lower than the values (all of the values of $R = 0.9996$) which obtained by the empirical VFT equation (see **Table 18**). So, the measurement electrical conductivity does not follow the Arrhenius Eq. (15). In **Figure 17**, it can also be seen that the measurement points lie far away from the fitted straight lines. The FILs [MCNMIM][NTf$_2$], [PCNMIM][NTf$_2$], [EOHMIM][NTf$_2$], and [CH$_2$CONHBuEIM][NTf$_2$] have also exhibited the same result.
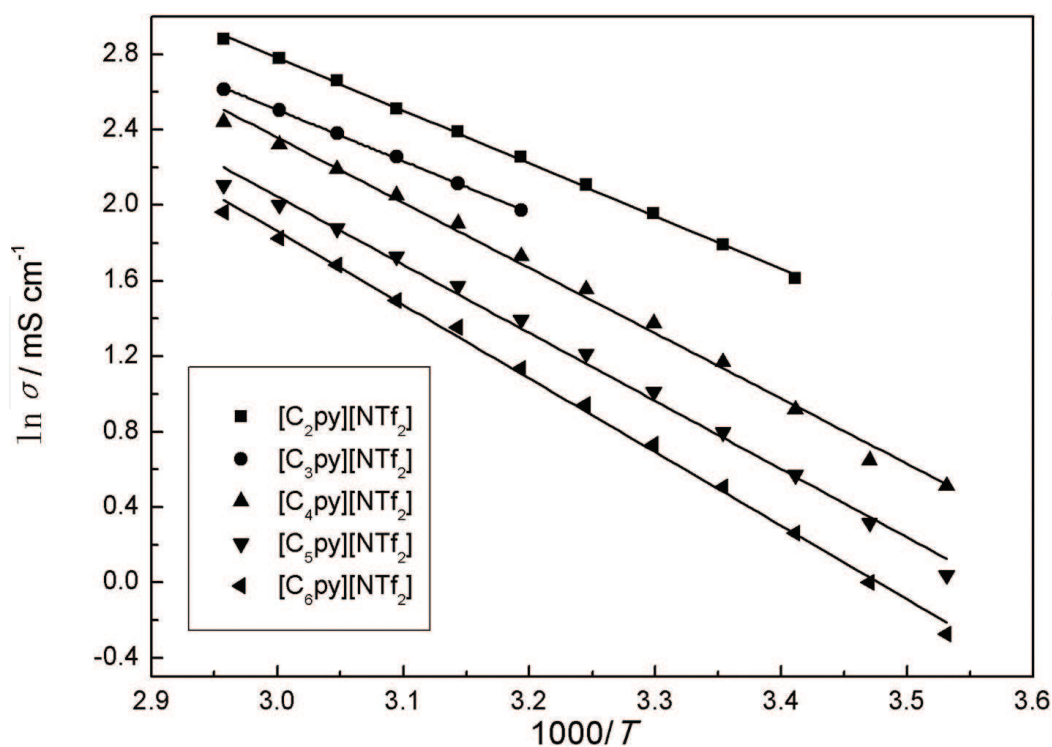

Figure 17. Plot of Ln σ vs. 1000/T of ILs [C$_n$py][NTf$_2$] ($n = 2, 3, 4, 5, 6$).

The Walden's product (in [S·cm²·mol⁻¹][mP·s]) can be calculated according to Eq. (17). The values are 60, 54, 48, 45 for $[C_2py][NTf_2]$, $[C_4py][NTf_2]$, $[C_5py][NTf_2]$, and $[C_6py][NTf_2]$ at 298.15 K, respectively. From the results, the values are decrease with the methylene introduced.

According to Eq. (17), the $\log\varLambda$ dependence on $\log\eta^{-1}$ is illustrated in **Figure 18** for the $[C_npy]$ $[NTf_2]$ ($n = 2, 3, 4, 5, 6$) from 283.15 to 338.15 K.
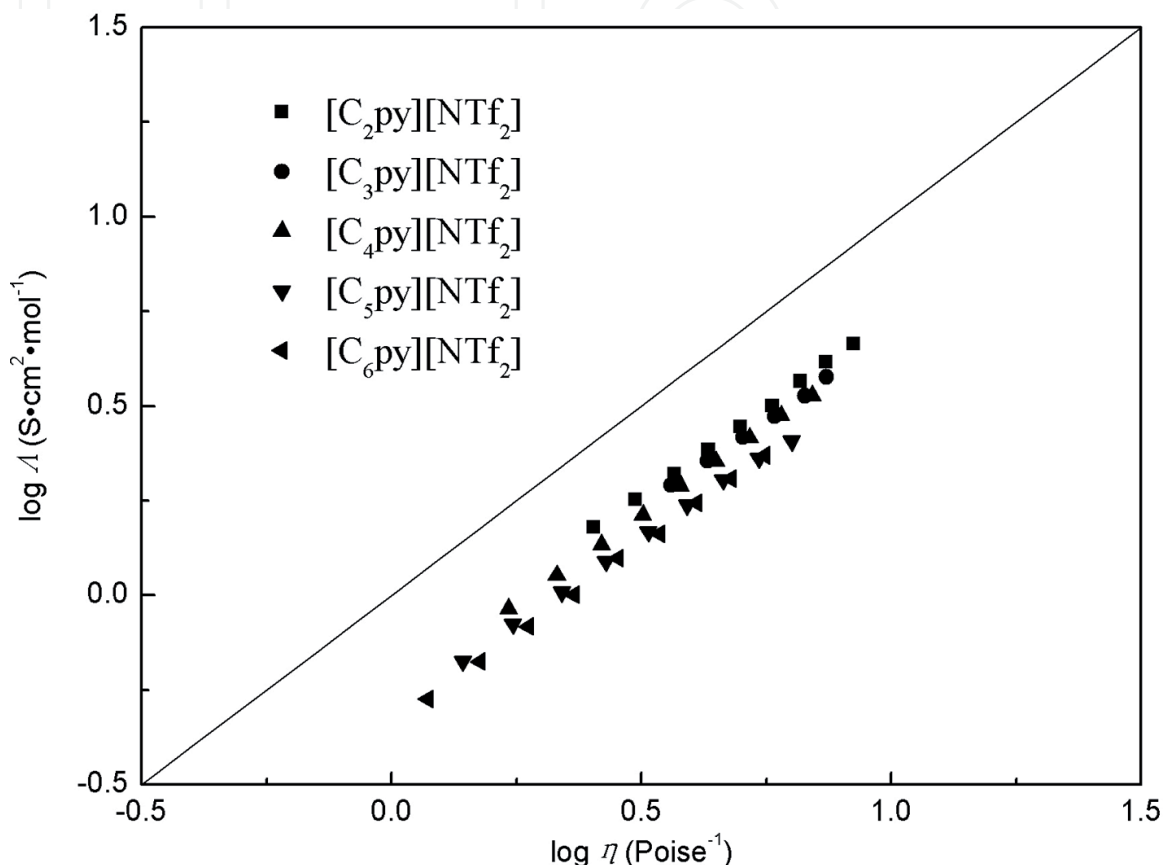

Figure 18. Walden plots for samples at temperature from 283.15 to 338.15 K for $[C_npy][NTf_2]$ ($n = 2, 3, 4, 5, 6$).

Usually, the Walden rule can be used for the presentation of the independent ions of the liquid. If the Walden points close to the ideal line, the liquid can be considered as a relative ideal liquid. The ideal line position was determined according to the aqueous KCl solution at high dilution. As an ideal line, the slop of the ideal line should be unity and not have any interaction of the ions [10, 29, 30]. In **Figure 10**, it can be seen that the approximately straight lines can be obtained according to the experimental points.

Like the FILs, the Walden rule can also be used for the presentation of the independent ions of the ILs $[C_npy][NTf_2]$ ($n = 2, 3, 4, 5, 6$). From **Figure 18**, it can be seen that the approximately straight lines can be obtained according to the experimental values. The fitted slopes of the lines for the ILs $[C_npy][NTf_2]$ ($n = 2, 3, 4, 5, 6$) are 0.941, 0.906, 0.935, 0.893, and 0.959, respectively. The lines for the ILs below are close to the ideal KCl line from **Figure 18**. Most of the reported traditional ILs [9, 10, 29–31] have the same tendency. Herein, the ILs $[C_npy]$

[NTf$_2$] (n = 2, 3, 4, 5, 6) can be called "subionic." It means that the ILs [C$_n$py][NTf$_2$] (n = 2, 3, 4, 5, 6) did not yield the expected conductivity from the high fluidities because on average the proton transfer is incomplete. The behavior of the ILs [C$_n$py][NTf$_2$] (n = 2, 3, 4, 5, 6) as if there is only a small population of ions and the "ionicity" of the ILs is therefore reduced [34].

8.2. N-Alkyl-3-methyl or N-alkyl-4-methyl type pyridinium-type ionic liquids

Two series ILs [C$_n$3Mpy][NTf$_2$] (n = 3, 4, 6) and [C$_n$4Mpy][NTf$_2$] (n = 2, 4, 6) were synthesized in this section. From **Figure 11**, the two series ILs introduced the methyl group on the pyridinium ring and the positions are position 3 and 4, respectively.

The values of the density, dynamic viscosity, and electrical conductivity are listed in **Tables 19–21** [27, 33, 45].

In order to compare the density, dynamic viscosity, and electrical conductivity with the N-alkyl type pyridinium-type ILs at 298.15 K, the values of the three series pyridinium-based ILs are listed in **Table 22**.

T/K	[C$_3$3mpy] [NTf$_2$]	[C$_4$3mpy] [NTf$_2$]	[C$_6$3mpy] [NTf$_2$]	[C$_2$4mpy] [NTf$_2$]	[C$_4$4mpy] [NTf$_2$]	[C$_6$4mpy] [NTf$_2$]
278.15	1.4685[c]	1.4399	1.3781[c]	1.5100[c]	1.4373[c]	1.3695[c]
283.15	1.4640[c]	1.4357	1.3736	1.5052	1.4328	1.3653
288.15	1.4596	1.4315	1.3697	1.5010	1.4284	1.3608
293.15	1.4556	1.4271	1.3653	1.4961	1.4234	1.3563
298.15	1.4514	1.4226	1.3615	1.4920	1.4187	1.3518
303.15	1.4471	1.4183	1.3570	1.4877	1.4140	1.3474
308.15	1.4426	1.4142	1.3529	1.4830	1.4093	1.3429
313.15	1.4380	1.4098	1.3487	1.4783	1.4047	1.3385
318.15	1.4332	1.4051	1.3447	1.4734	1.4002	1.3341
323.15	1.4287	1.4007	1.3403	1.4688	1.3958	1.3296
328.15	1.4245	1.3964	1.3360	1.4644	1.3913	1.3252
333.15	1.4203	1.3921	1.3317	1.4599	1.3869	1.3208
338.15	1.4160	1.3876	1.3280	1.4551	1.3825	1.3165
343.15	1.4113[c]	1.3832[c]	1.3237[c]	1.4506[c]	1.3777[c]	1.3121
348.15	1.4069[c]	1.3787[c]	1.3195[c]	1.4460[c]	1.3731[c]	1.3078
353.15	1.4025[c]	1.3742[c]	1.3154[c]	1.4414[c]	1.3686[c]	1.3034

Note: [c] calculated values.

Table 19. Experimental values of density, ρ, of two series ILs [C$_n$3Mpy][NTf$_2$] (n = 3, 4, 6) and [C$_n$4Mpy][NTf$_2$] (n = 2, 4, 6) at pressure p = 0.1 MPa.

T/K	[C$_3$3mpy] [NTf$_2$]	[C$_4$3mpy] [NTf$_2$]	[C$_6$3mpy] [NTf$_2$]	[C$_2$4mpy] [NTf$_2$]	[C$_4$4mpy] [NTf$_2$]	[C$_6$4mpy] [NTf$_2$]
278.15	160.80[c]	177.0[c]	276.16[c]	79.45[c]	159.65[c]	253.47[c]
283.15	118.12[c]	133.3[c]	199.61[c]	61.98[c]	118.57[c]	181.62
288.15	89.08[c]	102.3[c]	147.89[c]	49.30[c]	90.07[c]	133.92
293.15	68.73[c]	79.9[c]	112.00[c]	39.89[c]	69.82[c]	101.07
298.15	54.12	63.2	86.59	32.75	55.14	77.989
303.15	43.46	51.1	67.83	27.31	44.20	61.301
308.15	35.27	41.4	54.23	23.10	35.85	49.031
313.15	29.18	34.0	44.24	19.69	29.61	39.755
318.15	24.32	28.4	36.21	16.95	24.77	32.729
323.15	20.87	23.9	29.97	14.66	20.85	27.381
328.15	17.94	20.3	25.08	12.85	17.86	23.111
333.15	15.15	17.5	21.31	11.34	15.37	19.709
338.15	13.40	15.2	18.28	10.10	13.42	16.968
343.15	11.74	13.0	15.88	9.07	11.65	14.729
348.15	10.37	11.3	13.71	8.19	10.15	12.866
353.15	9.19	10.0	11.99	7.43	8.89	11.324
358.15				6.76	7.94	
363.15				6.19	7.20[c]	

Note: [c] calculated values.

Table 20. Experimental values of dynamic viscosity, η, of two series ILs [C$_n$3Mpy][NTf$_2$] (n = 3, 4, 6) and [C$_n$4Mpy][NTf$_2$] (n = 2, 4, 6) at pressure p = 0.1 MPa.

From **Table 22**, the density of the three series of pyridinium-type ILs decreases with the introduction of the methylene group on the alkyl side chain of the pyridinium-type ILs. The result is the same with the imidazolium-type ILs [12, 13]. The introduction of the methyl group on the pyridinium-type ILs leads the apparent decrease of the density. However, the degree of decreasing is different on the position 3 and 4 of the pyridinium ring. The introduction of the methyl group on position 4 leads the more decrease than position 3 on the pyridinium ring. The order is as follows: [C$_2$py][NTf$_2$] > [C$_2$4mpy][NTf$_2$]; [C$_4$py][NTf$_2$] > [C$_4$3mpy][NTf$_2$] > [C$_4$4mpy][NTf$_2$]; [C$_6$py][NTf$_2$] > [C$_6$3mpy][NTf$_2$] > [C$_6$4mpy][NTf$_2$].

As shown in **Table 22**, the electrical conductivity of the three series pyridinium-type ILs decreases with the introduction of the methylene group on the alkyl side chain of the pyridinium-type ILs. But, the introduction of the methyl group on the ring leads to the different change tendency for electrical conductivity. For density, the values are decrease with the introduction of the methyl group on positions 3 and 4 of the pyridinium ring. However, the electrical conductivity decreases after the introduction of methyl group on position 3 and increases after the introduction of the methyl group on position 4 of the pyridinium ring. The tendency is just the reverse and the order is as follow: [C$_2$py][NTf$_2$] < [C$_2$4mpy][NTf$_2$]; [C$_4$3mpy][NTf$_2$] < [C$_4$py][NTf$_2$] < [C$_4$4mpy][NTf$_2$]; [C$_6$3mpy][NTf$_2$] < [C$_6$py][NTf$_2$] < [C$_6$4mpy][NTf$_2$].

T/K	[$C_3$3mpy] [NTf$_2$]	[$C_4$3mpy] [NTf$_2$]	[$C_6$3mpy] [NTf$_2$]	[$C_2$4mpy] [NTf$_2$]	[$C_4$4mpy] [NTf$_2$]	[$C_6$4mpy] [NTf$_2$]
278.15	1.524	1.00	0.495	3.39[c]	1.24	0.592[c]
283.15	1.990	1.32	0.670	4.24	1.66	0.839
288.15	2.53	1.72	0.885	5.25	2.15	1.101
293.15	3.18	2.17	1.157	6.38	2.73	1.447
298.15	3.93	2.72	1.480	7.63	3.41	1.852
303.15	4.76	3.35	1.869	9.01	4.19	2.31
308.15	5.71	4.09	2.31	10.50	5.09	2.83
313.15	6.71	4.90	2.83	12.08	6.00	3.46
318.15	7.86	5.76	3.42	13.78	7.02	4.15
323.15	9.04	6.90	4.06	15.54	8.17	4.87
328.15	10.36	7.96	4.77	17.50	9.41	5.71
333.15	11.79	9.10	5.53	19.55	10.75	6.52
338.15	13.29	10.31	6.38	21.7	12.07	7.56
343.15	14.85	11.60	7.28	23.9[c]	13.56[c]	8.61
348.15	16.50	12.96	8.22	26.2[c]	15.10[c]	9.68
353.15	18.28	14.37	9.20	28.5[c]	16.70[c]	10.75

Note: [c] calculated values.

Table 21. Experimental values of electrical conductivity, σ, of two series ILs [C_n3Mpy][NTf$_2$] (n = 3, 4, 6) and [C_n4Mpy][NTf$_2$] (n = 2, 4, 6) at pressure p = 0.1 MPa.

	ρ/(g·cm^{-3})	η/(mPa·s)	σ/(mS·cm^{-1})
[C_2py][NTf$_2$]	1.5375	39.4	5.99
[C_4py][NTf$_2$]	1.4547	58.3	3.21
[C_5py][NTf$_2$]	1.4214	71.9	2.22
[C_6py][NTf$_2$]	1.3877	84.5	1.66
[$C_3$3mpy][NTf$_2$]	1.4514	54.12	3.93
[$C_4$3mpy][NTf$_2$]	1.4226	63.2	2.72
[$C_6$3mpy][NTf$_2$]	1.3615	86.59	1.480
[$C_2$4mpy][NTf$_2$]	1.4920	32.75	7.63
[$C_4$4mpy][NTf$_2$]	1.4187	55.14	3.41
[$C_6$4mpy][NTf$_2$]	1.3518	77.989	1.852

Table 22. The comparison of density, ρ, dynamic viscosity, η, and electrical conductivity, σ, of three series pyridinium-based ILs at 298.15 K and pressure p = 0.1 MPa.

For the dynamic viscosity, the values of the three series pyridinium-type ILs increase with the introduction of the methylene group on the alkyl side chain of pyridinium-type cation ILs. Like the electrical conductivity, the dynamic viscosity also exhibited the difference tendency with the density after the introduction of the methyl group on the pyridinium ring. However, the tendency is in contrast to the electrical conductivity. For dynamic viscosity, the values increase with the introduction of the methyl group on position 3 of the pyridinium ring and decrease with the introduction of the methyl group on position 4 of the pyridinium ring with the non-substituting pyridinium ring. The order is as follows: $[C_2py][NTf_2] > [C_24mpy][NTf_2]$; $[C_43mpy][NTf_2] > [C_4py][NTf_2] > [C_44mpy][NTf_2]$; $[C_63mpy][NTf_2] > [C_6py][NTf_2] > [C_64mpy][NTf_2]$.

According to **Table 19**, the temperature dependence of the density values can be plotted and fitted according to the linear equation (**Figure 19**).
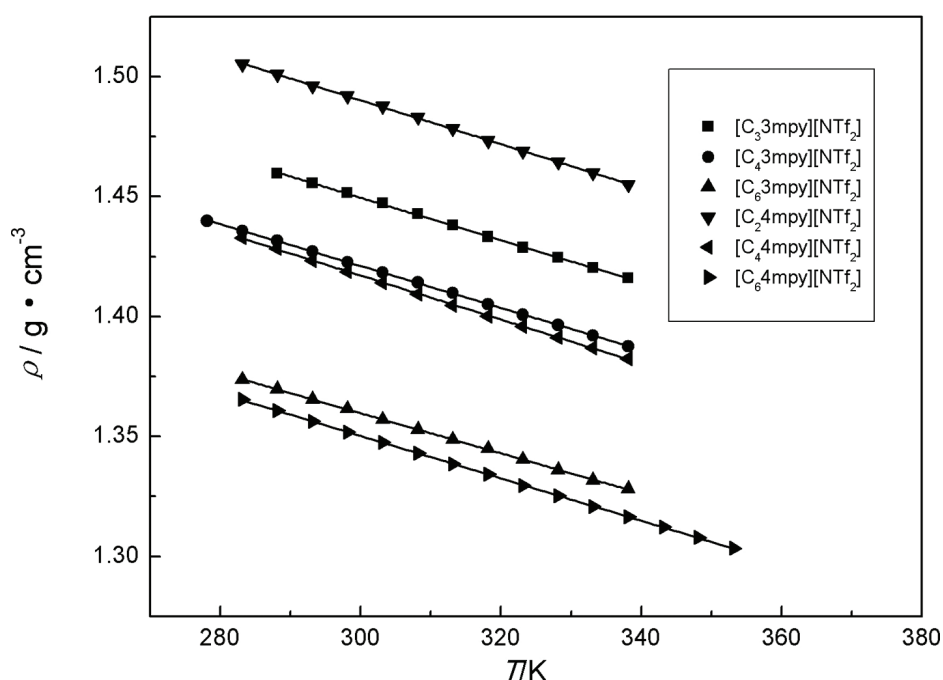

Figure 19. Plot of density, ρ, vs. temperature, T, for two series ILs $[C_n3Mpy][NTf_2]$ ($n = 3, 4, 6$) and $[C_n4Mpy][NTf_2]$ ($n = 2, 4, 6$).

The thermal expansion coefficient, α, molecular volume, V_m, standard molar entropy, S^0, and lattice energy, U_{POT}, were calculated from experimental density using the empirical Eqs. (1)–(4). The obtained data from the empirical equations are listed in **Table 23**.

From **Table 23**, the thermal expansion coefficients are 6.12×10^{-4} K^{-1} for $[C_33mpy][NTf_2]$, 6.20×10^{-4} K^{-1} for $[C_43mpy][NTf_2]$, 6.19×10^{-4} K^{-1} for $[C_63mpy][NTf_2]$, 6.17×10^{-4} K^{-1} for $[C_24mpy][NTf_2]$, 6.52×10^{-4} K^{-1} for $[C_44mpy][NTf_2]$, and 6.62×10^{-4} K^{-1} for $[C_64mpy][NTf_2]$, respectively. The values are in good agreement with the range of 5×10^{-4} to 7×10^{-4} K^{-1} obtained by Jacquemin et al. 44]. According to **Table 23**, the mean contributions of the methylene to the molecular volume are 0.0277 nm^3 for $[C_n3mpy][NTf_2]$ ($n = 3, 4, 6$) and 0.0289 nm^3 for $[C_n4mpy][NTf_2]$ ($n = 2, 4, 6$) at 298.15 K. The values are in good agreement with the values of 0.0280 nm^3 for ILs $[C_npy][NTf_2]$ [4, 26].

From **Table 20**, the temperature dependence on dynamic viscosity can be fitted according to VFT Eq. (11), see **Figure 20**.

Property	[C$_3$3mpy] [NTf$_2$]	[C$_4$3mpy] [NTf$_2$]	[C$_6$3mpy] [NTf$_2$]	[C$_2$4mpy] [NTf$_2$]	[C$_4$4mpy] [NTf$_2$]	[C$_6$4mpy] [NTf$_2$]
MW/(g·mol^{-1})	416.35	430.38	458.43	402.33	430.38	458.43
V_m/(nm^3)	0.4765	0.5025	0.5593	0.4479	0.5039	0.5633
$10^4\alpha$/(K^{-1})	6.12	6.20	6.19	6.17	6.52	6.62
V/(cm^{-3}·mol^{-1})	286.9	302.5	336.7	269.7	303.4	339.1
S^0/(J·K^{-1}·mol^{-1})	623.5	655.9	726.7	587.8	657.6	731.7
U_{pot}/(kJ·mol^{-1})	404	399	389	410	399	388

Table 23. Estimated values of physicochemical properties of two series pyridinium-based ILs at 298.15 K.
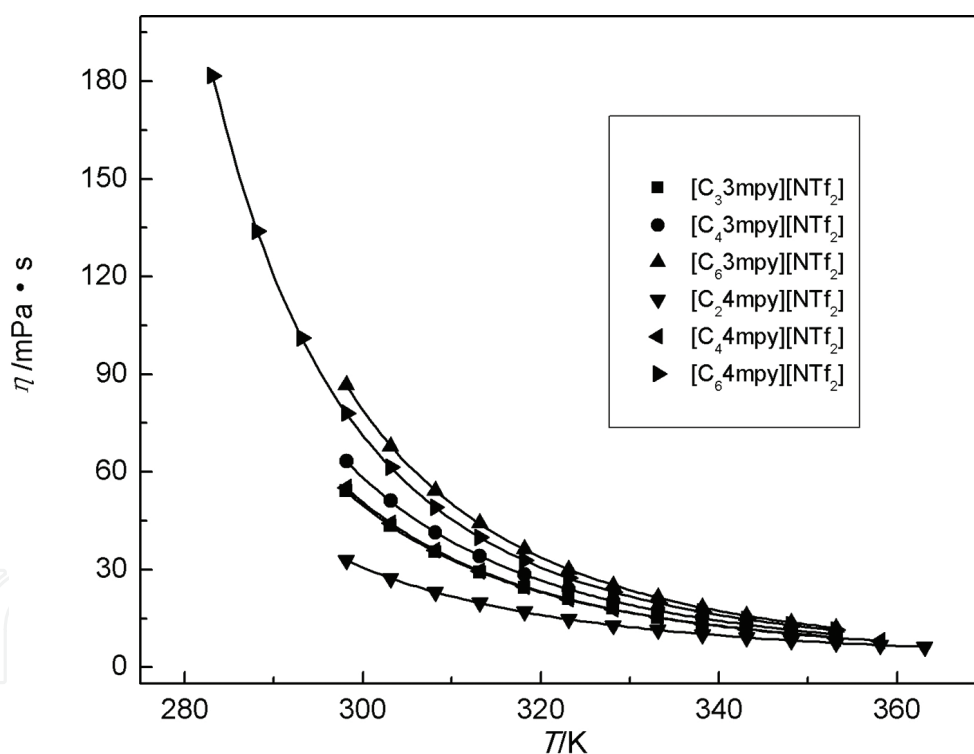
Figure 20. Plot of dynamic viscosity, η, vs. temperature, T, for two series ILs [C$_n$3Mpy][NTf$_2$] (n = 3, 4, 6) and [C$_n$4Mpy][NTf$_2$] (n = 2, 4, 6).

The best-fitting parameters of η_0, B, T_0, and the corresponding correlation coefficient, R, are listed in **Table 24**. From **Table 24**, the obtained values of the correlation coefficient, R, are higher than 0.9999, which indicates that the VFT equation can be used for fitting the experimental dynamic viscosity.

According to Eq. (13), the activation energies of dynamic viscosity for the two series ILs [C$_n$3Mpy] [NTf$_2$] (n = 3, 4, 6) and [C$_n$4Mpy][NTf$_2$] (n = 2, 4, 6) were calculated and are listed in **Table 24**.

The 1000 T^{-1} dependence on Ln η was plotted for the ILs [C$_n$3Mpy][NTf$_2$] (n = 3, 4, 6) and [C$_n$4Mpy][NTf$_2$] (n = 2, 4, 6) (see **Figure 21**) according to Eq. (12).

Property	[C$_3$3mpy] [NTf$_2$]	[C$_4$3mpy] [NTf$_2$]	[C$_6$3mpy] [NTf$_2$]	[C$_2$4mpy] [NTf$_2$]	[C$_4$4mpy] [NTf$_2$]	[C$_6$4mpy] [NTf$_2$]
η_0/(mPa·s)	0.1523	0.0474	0.0749	0.1768	0.0859	0.1170
B/K	751.0	1151.7	997.9	720.6	914.6	847.2
$10^3 E_\eta$/eV	64.8	99.4	86.1	62.2	79.9	73.1
T_0/K	170.3	138.1	156.6	160.2	156.6	167.9
R^2	0.99999	0.9999	0.99999	0.99997	0.99996	0.99999

Table 24. Fitted parameter values of η_0, B, T_0, and correlation coefficient, R^2, by Eq. (**11**) and $E\eta$ by Eq. (**13**).
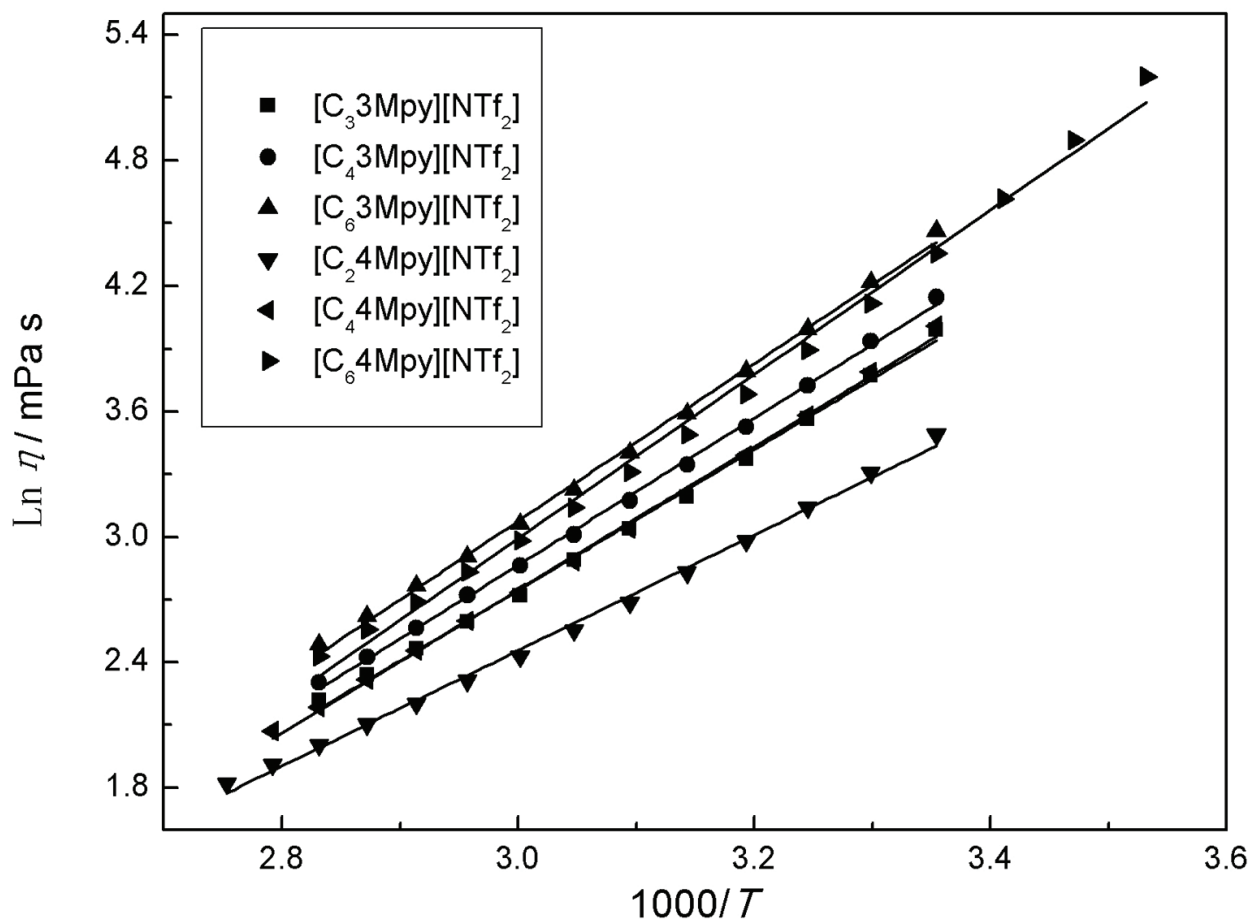
Figure 21. Plot of Ln η vs. 1000/T of ILs [C$_n$3Mpy][NTf$_2$] (n = 3, 4, 6) and [C$_n$4Mpy][NTf$_2$] (n = 2, 4, 6).

In **Figure 21**, the 1000/T dependences on ln η of the two ILs [C$_n$3Mpy][NTf$_2$] (n = 3, 4, 6) and [C$_n$4Mpy][NTf$_2$] (n = 2, 4, 6) were fitted in the temperature range. The values of the correlation coefficient, R, are 0.9972, 0.9987, 0.9978, 0.9966, 0.9981, and 0.9947, respectively. The values are much lower than the values (all of the values are higher than R = 0.9999) which fitted according to the empirical VFT equation (see **Table 24**). So, the measurement dynamic viscosity cannot be well fitted with the Arrhenius Eq. (12). From **Figure 21**, it can also be obviously obtained that the measurement points lie far away from the straight fitting lines. The FILs [MCNMIM][NTf$_2$], [PCNMIM][NTf$_2$], [EOHMIM][NTf$_2$], and [CH$_2$CONHBuEIM][NTf$_2$] have also exhibited the same result.

From **Table 21**, the temperature dependence on electrical conductivity can be fitted according to VFT Eq. (14), see **Figure 22**.
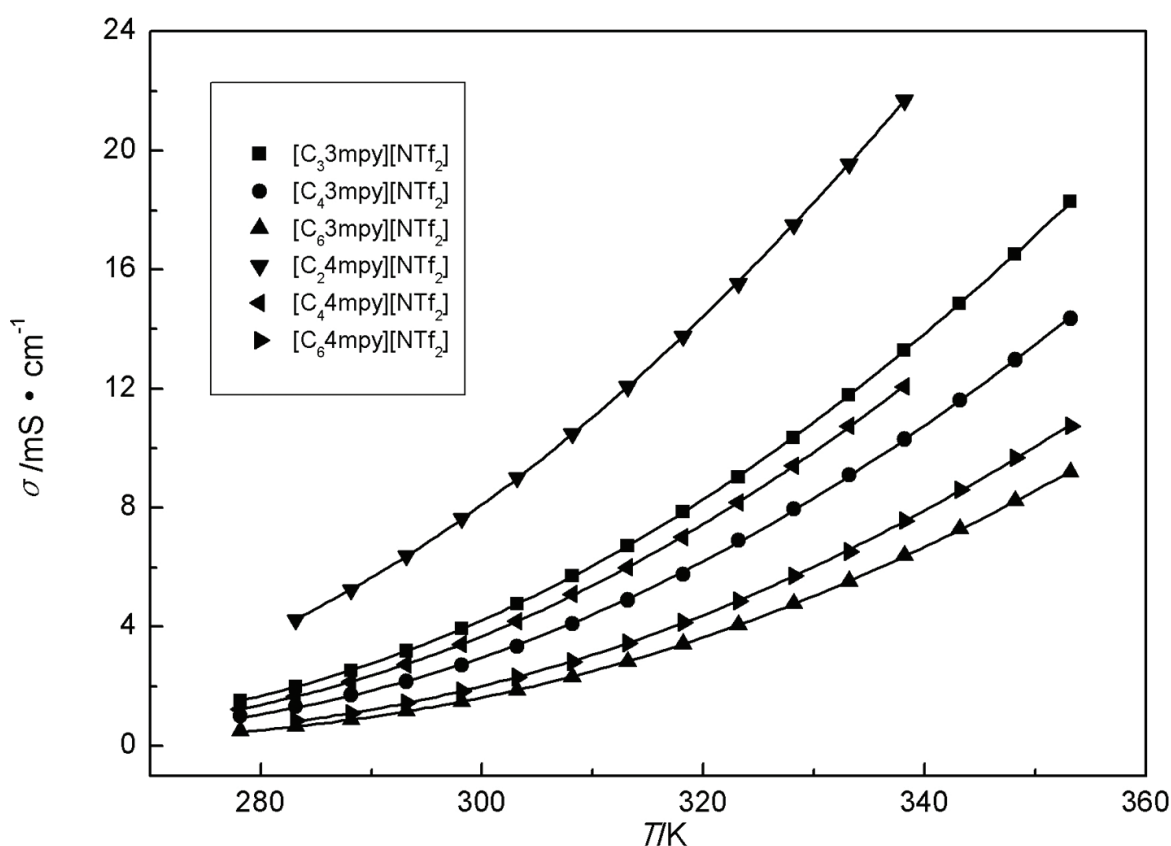
Figure 22. Plot of electrical conductivity, σ, vs. temperature, T, of two ILs [C$_n$3Mpy][NTf$_2$] (n = 3, 4, 6) and [C$_n$4Mpy] [NTf$_2$] (n = 2, 4, 6).

The best-fitting parameters of σ_0, B, T_0, and the corresponding correlation coefficient, R, are listed in **Table 25**. From **Table 25**, the obtained values of the correlation coefficient, R, are higher than 0.9999, which indicates that the VFT equation can be used for fitting the experimental electrical conductivity.

The activation energies of electrical conductivity for the two series ILs $[C_n3Mpy][NTf_2]$ ($n = 3, 4, 6$) and $[C_n4Mpy][NTf_2]$ ($n = 2, 4, 6$) were calculated by Eq. (16) and are listed in **Table 25**.

The $1000/T$ dependence on $\ln \sigma$ was plotted for the two series ILs $[C_n3Mpy][NTf_2]$ ($n = 3, 4, 6$) and $[C_n4Mpy][NTf_2]$ ($n = 2, 4, 6$) (see **Figure 23**) by Eq. (15).

Property	$[C_33mpy][NTf_2]$	$[C_43mpy][NTf_2]$	$[C_63mpy][NTf_2]$	$[C_24mpy][NTf_2]$	$[C_44mpy][NTf_2]$	$[C_64mpy][NTf_2]$
$\sigma_0/(S\cdot cm^{-1})$	0.64	0.49	0.47	0.64	0.50	0.46
B/K	650.2	608.4	684.6	574.6	586.5	647.3
$10^3E_\sigma/eV$	56.1	52.4	59.0	49.5	50.6	55.9
T_0/K	170.7	181.0	179.3	168.5	180.4	181.0
R^2	0.99996	0.9999	0.99992	0.99997	0.99996	0.99999

Table 25. Fitted parameter values of σ_0, B, T_0, and correlation coefficient, R^2, by Eq. (**15**) and E_σ by Eq. (**17**).
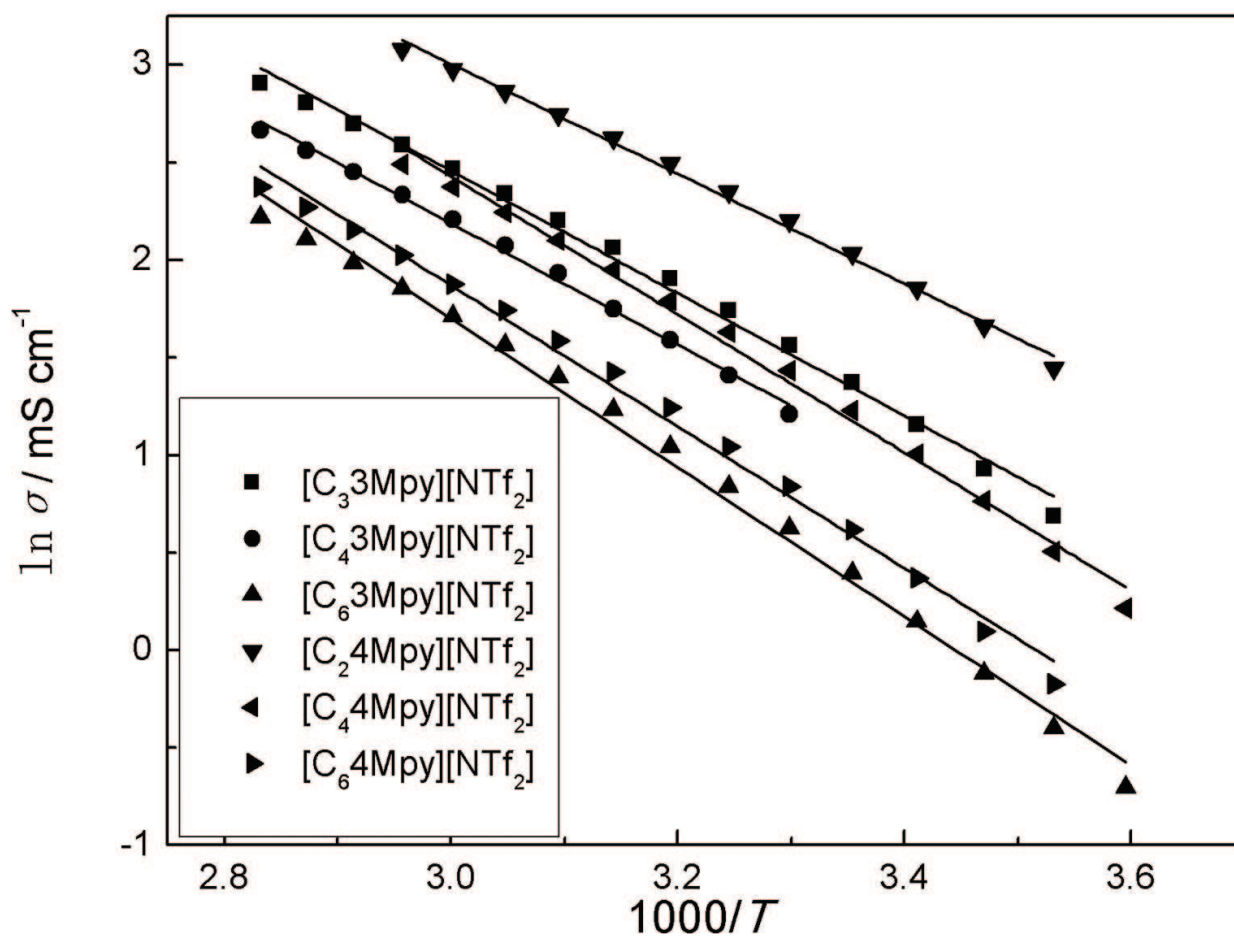
Figure 23. Plot of Ln σ vs. $1000/T$ of ILs for the two series ILs $[C_n3Mpy][NTf_2]$ ($n = 3, 4, 6$) and $[C_n4Mpy][NTf_2]$ ($n = 2, 4, 6$).

In **Figure 23**, the $1000/T$ dependence on ln σ of the two ILs [C$_n$3Mpy][NTf$_2$] (n = 3, 4, 6) and [C$_n$4Mpy][NTf$_2$] (n = 2, 4, 6) was fitted in the temperature range. The values of the correlation coefficient, R, are 0.9957, 0.9935, 0.9933, 0.9943, 0.9958, and 0.9936, respectively. The values are much lower than the values (all of the values are higher than R = 0.9999) which fitted by the empirical VFT equation (see **Table 25**). So, the measurement values cannot be well fitted with the Arrhenius Eq. (15). From **Figure 23**, the measurement points can also be obviously shown far away from the straight fitting lines. The FILs [MCNMIM][NTf$_2$], [PCNMIM][NTf$_2$], [EOHMIM][NTf$_2$], and [CH$_2$CONHBuEIM][NTf$_2$] have also exhibited the same result.

According to Eq. (17), the Walden products (in [S·cm^2·mol^{-1}][cP]) are calculated and the values are 61 for [C$_3$3mpy][NTf$_2$], 52 for [C$_4$3mpy][NTf$_2$], 43 for [C$_6$3mpy][NTf$_2$], 67 for [C$_2$4mpy][NTf$_2$], 53 for [C$_4$4mpy][NTf$_2$], and 49 for [C$_6$4mpy][NTf$_2$] at 298.15 K. From the results we found that the values are also decrease with the introduction of the methylene group such as the N-alkyl pyridinium-type ILs.

Log Λ dependence on log η^{-1} was plotted for the ILs [C$_n$3mpy][NTf$_2$] (n = 3, 4, 6) and [C$_n$4mpy][NTf$_2$] (n = 2, 4, 6) from 273.15 to 353.15 K according to Eq. (17) (see **Figure 24**).
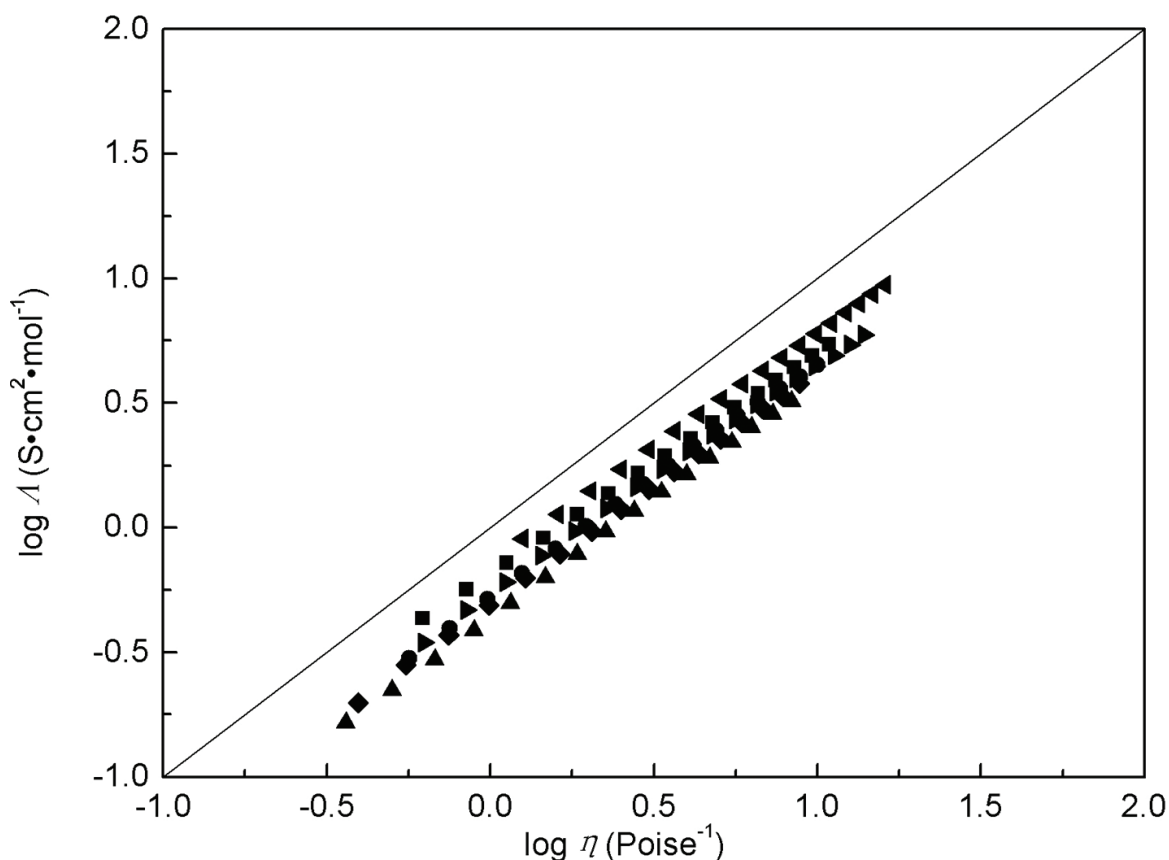

Figure 24. Walden plots for samples at temperature from 273.15 to 353.15 K.

From **Figure 24**, it can be observed that the curves are approximately straight lines. The slopes of the lines for the ILs $[C_n3mpy][NTf_2]$ (n = 3, 4, 6) and $[C_n4mpy][NTf_2]$ (n = 2, 4, 6) are 0.887, 0.949, 0.954, 0.915, 0.912, and 0.946, respectively. The position of the ideal line was established using aqueous KCl solutions at high dilution. The lines of the ILs $[C_n3mpy]$ $[NTf_2]$ (n = 3, 4, 6) and $[C_n4mpy][NTf_2]$ (n = 2, 4, 6) lie below and closely to the ideal KCl line. The ILs $[C_n3mpy][NTf_2]$ (n = 3, 4, 6) and $[C_n4mpy][NTf_2]$ (n = 2, 4, 6) are "subionic" [38].

Conclusion

The density, surface tension, dynamic viscosity, and electrical conductivity of the three series hydrophobic pyridinium-type ILs $[C_npy][NTf_2]$ (n = 2, 3, 4, 5, 6), $[C_n3Mpy][NTf_2]$ (n = 3, 4, 6), and $[C_n4Mpy][NTf_2]$ (n = 2, 4, 6) were determined at atmospheric pressure in the temperature range of 278–363 K. The thermal expansion coefficient, molecular volume, standard molar entropy, and lattice energy of the samples were estimated in terms of empirical and semiempirical equations. The density and electrical conductivity decrease with the introduction of the methylene group on the alkyl side chain of the pyridinium type. However, the dynamic viscosity exhibited the inverse tendency. Compared with the methylene group, the introduction of the methyl group on the pyridinium ring exhibited the irregular tendency to the density, dynamic viscosity and electrical conductivity. The order is as follows: $[C_24mpy][NTf_2] < [C_2py][NTf_2]$, $[C_44mpy][NTf_2] < [C_43mpy][NTf_2] < [C_4py][NTf_2]$, and $[C_64mpy][NTf_2] < [C_63mpy][NTf_2] < [C_6py][NTf_2]$ for density; $[C_24mpy][NTf_2] < [C_2py][NTf_2]$, $[C_44mpy][NTf_2] < [C_4py][NTf_2] < [C_43mpy][NTf_2]$, and $[C_64mpy][NTf_2] < [C_6py][NTf_2] < [C_63mpy][NTf_2]$ for dynamic viscosity; $[C_24mpy][NTf_2] > [C_2py][NTf_2]$, $[C_44mpy][NTf_2] > [C_4py][NTf_2] > [C_43mpy][NTf_2]$, and $[C_64mpy][NTf_2] > [C_6py][NTf_2] > [C_63mpy][NTf_2]$ for electrical conductivity. According to the correlation coefficients, the empirical equation can be satisfactorily used for the fitting of the dynamic viscosity and electrical conductivity of the pyridinium-type ILs. However, the Arrhenius equation cannot be used for the fitting of the measurement values.

Author details

Liu Qingshan*, Mou Lin, Zheng Qige and Xia Quan

*Address all correspondence to: 13478787524@163.com

Shenyang Agriculture University, College of Science, Shenyang, Liaoning, P. R. China

References

[1] J. Fuller, R. T. Carlin. Structural and Electrochemical Characterization of 1,3-bis-(4-methylphenyl)imidazolium Chloride. J. Chem. Crystallogr. 1994;24(8):489–493. DOI: 10.1007/ BF01666725

[2] C. M. Gordon, J. D. Holbrey, A. R. Kennedy, K. R. Seddon. Ionic Liquid Crystals: Hexafluorophosphate Salts. J. Mater. Chem. 1998;8(12):2627–2636. DOI: 10.1039/A806169F

[3] P. Bonhôte, A. P. Dias, N. Papageorgiou, K. Kalyanasundaram, M. Grätzel. Hydrophobic, Highly Conductive Ambient-Temperature Molten Salts. Inorg. Chem. 1996;35(5):1168–1178. DOI: 10.1021/ic951325x

[4] Q. S. Liu, M. Yang, P. F. Yan, X. M. Liu, Z.C. Tan, U. W. Biermann. Density and Surface Tension of Ionic Liquids $[C_n py][NTf_2]$ (n = 2, 4, 5). J. Chem. Eng. Data. 2010;55(11):4928–4930. DOI: 10.1021/je100507n

[5] H. Li, Z. Li, J. Yin, C. Li, Y. Chi, Q. Liu, X. Zhang, U. W. Biermann. Liquid-Liquid Extraction Process of Amino Acids by a New Amide-Based Functionalized Ionic Liquid. Green Chem. 2012;14(6):1721–1727. DOI: 10.1039/C2GC16560K

[6] J. Z. Yang, X. M. Lu, J. S. Gui, W. G. Xu. A New Theory for Ionic Liquids—The Interstice Model Part 1. The Density and Surface Tension of Ionic Liquid EMISE. Green Chem. 2004;6(11):541–543. DOI: 10.1039/B412286K

[7] Q. G. Zhang, J. Z. Yang, X. M. Lu, J. S. Gui, M. Huang. Studies on an Ionic Liquid Based on FeCl3 and its Properties. Fluid Phase Equilib. 2004;226(1):207–211. DOI: 10.1016/j.fluid.2004.09.020

[8] J. Vila, P. Ginés, J. M. Pico, C. Franjo, E. Jiménez, L. M. Varela, O. Cabeza. Temperature Dependence of the Electrical Conductivity in EMIM-Based Ionic Liquids: Evidence of Vogel-Tamman-Fulcher Behavior. Fluid Phase Equilib. 2006;242(2):141–146. DOI: 10.1016/j.fluid.2006.01.022

[9] M. Yoshizawa, W. Xu, C. A. Angell. Ionic Liquids by Proton Transfer: Vapor Pressure, Conductivity, and the Relevance of $\Delta_p K_a$ from Aqueous Solutions. J. Am. Chem. Soc. 2003;125(50):15411–15419. DOI: 10.1021/ja035783d

[10] W. Xu, E. I. Cooper, C. A. Angell. Ionic Liquids: Ion Mobilities, Glass Temperatures, and Fragilities. J. Phys. Chem. B. 2003;107(25):6170–6178. DOI: 10.1021/jp0275894

[11] Q. S. Liu, J. Tong, Z. C. Tan, U. W. Biermann, J. Z. Yang. Density and Surface Tension of Ionic Liquid $[C_2mim][PF_3(CF_2CF_3)_3]$ and Prediction of Properties $[C_nmim][PF_3(CF_2CF_3)_3]$ (n = 1, 3, 4, 5, 6). J. Chem. Eng. Data. 2010;55(7):2586–2589. DOI: 10.1021/je901035d

[12] J. Tong, Q. S. Liu, W. G. Xu, D. W. Fang, J. Z. Yang. Estimation of Physicochemical Properties of Ionic Liquids 1-Alkyl-3-Methylimidazolium Chloroaluminate. J. Phys. Chem. B. 2008;112(14):4381–4386. DOI: 10.1021/jp711767z

[13] D. W. Fang, W. Guan, J. Tong, Z. W. Wang, J. Z. Yang. Study on Physicochemical Properties of Ionic Liquids Based on Alanine $[C_nmim][Ala]$ (n = 2, 3, 4, 5, 6). J. Phys. Chem. B. 2008;112(25):7499–7505. DOI: 10.1021/jp801269u

[14] M. Egashira, S. Okada, J. I. Yamaki, D. A. Dri, F. Bonadies, B. Scrosati. The Preparation of Quaternary Ammonium-Based Ionic Liquid Containing a Cyano Group and its Properties in a Lithium Battery Electrolyte. J. Power Sources. 2004;138(1–2):240–244. DOI: 10.1016/j.jpowsour.2004.06.022

[15]   M. Egashira, H. Todo, N. Yoshimoto, M. Morita, J. I. Yamaki. Functionalized Imidazolium Ionic Liquids as Electrolyte Components of Lithium Batteries. J. Power Sources. 2007;174(2):560–564. DOI: 10.1016/j.jpowsour.2007.06.123

[16]   M. Egashira, M. Nakagawa, I. Watanabe, S. Okada, J. I. Yamaki. Cyano-Containing Quaternary Ammonium-Based Ionic Liquid as a 'Co-Solvent' for Lithium Battery Electrolyte. J. Power Sources. 2005;146(1–2):685–688. DOI: 10.1016/j.jpowsour.2005.03.069

[17]   C. Hardacre, J. D. Holbrey, C. L. Mullan, M. Nieuwenhuyzen, W. M. Reichert, K. R. Seddon, S. J. Teat. Ionic Liquid Characteristics of 1-Alkyl-N-Cyanopyridinium and 1-Alkyl-N-(Trifluoromethyl)pyridinium Salts. New J. Chem. 2008;32(11):1953–1967. DOI: 10.1039/B805063E

[18]   C. Hardacre, J. D. Holbrey, C. L. Mullan, M. Nieuwenhuyzen, T. G. A. Youngs, D. T. Bowronb, S. J. Teat. Solid and Liquid Charge-Transfer Complex Formation Between 1-Methylnaphthalene and 1-Alkyl-Cyanopyridinium Bis{(trifluoromethyl)sulfonyl} imide Ionic Liquids. Phys. Chem. Chem. Phys. 2010;12(8):1842–1853. DOI: 10.1039/ B921160H

[19]   J. Zhang, Q. Zhang, B. Qiao, Y. Deng. Solubilities of the Gaseous and Liquid Solutes and Their Thermodynamics of Solubilization in the Novel Room-Temperature Ionic Liquids at Infinite Dilution by Gas Chromatography. J. Chem. Eng. Data. 2007;52(6):2277–2283. DOI: 10.1021/je700297c

[20]   E. D. Bates, R. D. Mayton, I. Ntai, J. H. Davis, Jr. CO_2 Capture by a Task-Specific Ionic Liquid. J. Am. Chem. Soc. 2002;124(6):926–927. DOI: 10.1021/ja017593d

[21]   Y. Cai, Y. Peng. Amino-Functionalized Ionic Liquid as an Efficient and Recyclable Catalyst for Knoevenagel Reactions in Water. Catal. Lett. 2006;109(1):61–64. DOI: 10.1007/ s10562–006–0057–3

[22]   S. Hu, T. Jiang, Z. Zhang, A. Zhu, B. Han, J. Song, Y. Xie, W. Li. Functional Ionic Liquid from Biorenewable Materials: Synthesis and Application as a Catalyst in Direct Aldol Reactions. Tetrahedron Lett. 2007;48(32):5613–5617. DOI: 10.1016/j.tetlet.2007.06.051

[23]   Q-S. Liu, J. Liu, X-X. Liu, S-T. Zhang. Density, Dynamic Viscosity, and Electrical Conductivity of Two Hydrophobic Functionalized Ionic Liquids. J. Chem. Thermodyn. 2015;90:39–45. DOI: 10.1016/j.jct.2015.06.010

[24]   Q. S. Liu, Z. Li, U. W. Biermann, C. P. Li, X. Liu. Thermodynamic Properties of a New Hydrophobic Amide-Based Task-Specific Ionic Liquid [$EimCH_2CONHBu$][NTf_2]. J. Chem. Eng. Data. 2013;58(1):93–98. DOI: 10.1021/je301001g

[25]   Q. S. Liu, H. Liu, L. Mou. Properties of 1-(Cyanopropyl)-3-Methylimidazolium Bis[(trifluoromethyl)sulfonyl]imide. Acta. Phys. Chim. Sin. 2016;32(3):617–623. DOI: 10.3866/PKU.WHXB201512171

[26]   Q. S. Liu, M. Yang, P. P. Li, S-S. Sun, U. W. Biermann, Z-C. Tan, Q-G. Zhang. Physicochemical Properties of Ionic Liquids [C_3py][NTf_2] and [C_6py][NTf_2]. J. Chem. Eng. Data. 2011;56(11):4094–4101. DOI: 10.1021/je200534b

[27] Q. S. Liu, P. P. Li, U. W. Biermann, J. Chen, X. Liu. Density, Dynamic Viscosity, and Electrical Conductivity of Pyridinium-based Hydrophobic Ionic Liquids. J. Chem. Thermodyn. 2013;66:88–94. DOI: 10.1016/j.jct.2013.06.008

[28] D. R. Lide. Handbook of Chemistry and Physics. 84th ed. U.S.A: LLC; 2003–2004. 2616 p. ISBN: 0–8493–0484–9

[29] C. A. Angell, N. Byrne, J. P. Belieres. Parallel Developments in Aprotic and Protic Ionic Liquids: Physical Chemistry and Applications. Acc. Chem. Res. 2007;40(11):1228–1236. DOI: 10.1021/ar7001842

[30] D. R. MacFarlane, M. Forsyth, E. I. Izgorodina, A. P. Abbott, G. Annat, K. Fraser. On the Concept of Ionicity in Ionic Liquids. Phys. Chem. Chem. Phys. 2009;11(25):4962–4967. DOI: 10.1039/B900201D

[31] K. Matsumoto, R. Hagiwara. A New Series of Ionic Liquids Based on the Difluorophosphate Anion. Inorg. Chem. 2009;48(15):7350–7358. DOI: 10.1021/ic9008009

[32] Q. S. Liu, P. F. Yan, M. Yang, Z. C. Tan, C. P. Li, U. W. Biermann. Dynamic Viscosity and Conductivity of Ionic Liquids $[C_n py][NTf_2]$ (n = 2, 4, 5). Acta. Phys. Chim. Sin. 2011;27(12):2762–2766. DOI: 10.3866/PKU.WHXB20112762

[33] Q. S. Liu, P. P Li, U. W Biermann, X. X. Liu, J. Chen. Density, Electrical Conductivity, and Dynamic Viscosity of N-Alkyl-4-Methylpyridinium Bis(trifluoromethylsulfonyl)imide. J. Chem. Eng. Data 2012;57(11):2999–3004. DOI: 10.1021/je3004645

[34] J. P. Belieres, C. A. Angell. Protic Ionic Liquids: Preparation, Characterization, and Proton Free Energy Level Representation. J. Phys. Chem. B. 2007;111(18):4926–4937. DOI: 10.1021/jp067589u

[35] G. T. Kim, G. B. Appetecchi, F. Alessandrini, S. Passerini. Solvent-Free, PYR1ATFSI Ionic Liquid-Based Ternary Polymer Electrolyte Systems: I. Electrochemical Characterization. J. Power Sources. 2007;171(2):861–869. DOI: 10.1016/j.jpowsour.2007.07.020

[36] O. K. Kamijima, M. Yoshida, L. Yang. Application of Sulfonium-, Thiophenium-, and Thioxonium-Based Salts as Electric Double-layer Capacitor Electrolytes. J. Power Sources. 2010;195(19):6970–6976. DOI: 10.1016/j.jpowsour.2010.04.028

[37] M. Lazzari, M. Mastragostino, A. G. Pandolfo, V. Ruiz, F. Soavi. Role of Carbon Porosity and Ion Size in the Development of Ionic Liquid Based Supercapacitors. J. Electrochem. Soc. 2011;158(1):A22–A25. DOI: 10.1149/1.3514694

[38] H. Tokuda, S. Tsuzuki, M. A. B. H. Susan, K. Hayamizu, M. Watanabe. How Ionic Are Room-Temperature Ionic Liquids? An Indicator of the Physicochemical Properties. J. Phys. Chem. B. 2006;110(39):19593–19600. DOI: 10.1021/jp064159v

[39] F. S. Oliveira, M. G. Freire, P. J. Carvalho, J. A. P. Coutinho, J. N. Canongia Lopes, L. P. N. Rebelo, I. M. Marrucho. Structural and Positional Isomerism Influence in the Physical Properties of Pyridinium NTf_2-Based Ionic Liquids: Pure and Water-Saturated Mixtures. J. Chem. Eng. Data. 2010;55(10):4514–4520. DOI: 10.1021/je100377k

[40] J. Jacquemin, P. Husson, A. A. H. Padua, V. Majer. Density and Viscosity of Several Pure and Water-Saturated Ionic Liquids. Green Chem. 2006;8(2):172–180. DOI: 10.1039/B513231B

[41] A. Seduraman, P. Wu, M. Klähn. Extraction of Tryptophan with Ionic Liquids Studied with Molecular Dynamics Simulations. J. Phys. Chem. B. 2012;116(1):296–304. DOI: 10.1021/jp206748z

[42] J. Tong, M. Hong, W. Guan, J. B. Li, J. Z. Yang. Studies on the Thermodynamic Properties of New Ionic Liquids: 1-Methyl-3-Pentylimidazolium Salts Containing Metal of Group III. J. Chem. Thermodyn. 2006;38(11):1416–1421. DOI: 10.1016/j.jct.2006.01.017

[43] J. Tong, Q. Liu, W. Guan, J. Yang. Estimation of Physicochemical Properties of Ionic Liquid $C_6MIGaCl_4$ Using Surface Tension and Density. J. Phys. Chem. B. 2007;111(12):3197–200. DOI: 10.1021/jp068793k

[44] L. P. N. Rebelo, J. N. C. Lopes, J. M. S. S. Esperança, E. Filipe. On the Critical Temperature, Normal Boiling Point, and Vapor Pressure of Ionic Liquids. J. Phys. Chem. B. 2005;109(13):6040–6043. DOI: 10.1021/jp050430h

[45] Q. G. Zhang, Y. Wei, S. S. Sun, C. Wang, M. Yang, Q. S. Liu, Y. A. Gao. Study on Thermodynamic Properties of Ionic Liquid N-Butyl-3-Methylpyridinium Bis(trifluoromethylsulfonyl)imide. J. Chem. Eng. Data. 2012;57(8):2185–2190. DOI: 10.1021/je300153f